Joint Access and Relay-Assisted Backhaul Resource Allocation for Dense mmWave Multiple Access Networks

Jinsong Gui, Long Yin, Xiaoheng Deng, *Senior Member, IEEE*, and Lin Cai, *Fellow, IEEE*

***Abstract*—In dense millimeter wave (mmWave) multiple access networks, there are a large number of wireless access links and wireless backhaul links. The mmWave bandwidth is shared among two types of links. So a time-division mode is appropriate for such a scenario to determine a reasonable backhaul/access transmission duration, which is critical to network performance. Meanwhile, minimizing energy consumption is also an important design objective. However, the existence of long backhaul links is an obstacle. The introduction of relay mode can overcome it, but it also leads to more complex mutual interference relationships. On the other hand, each individual (e.g., smart wireless device) wants to obtain the highest access data rate, but it may prevent the entire network from achieving the highest energy efficiency. To cope with these challenges, we propose the new mutual interference characterization method and model the joint access and relay-assisted backhaul resource allocation problem as a Stackelberg game. The Stackelberg Nash equilibrium is guaranteed by the rational design of utility function, and the corresponding solution is solved by a backward induction method. Simulation results show that, our scheme is superior to the state-of-the-art in terms of network sum rate and network energy efficiency, and also it achieves a better balance between the access data rate and backhaul data rate for each access point.**

***Index Terms*—Multiple access networks, wireless resource allocation, network energy efficiency, stackelberg game.**

I. Introduction

TO MEET the exponential growth in access demands from a massive number of Internet of Things (IoT) devices [1], [2], dense deployment of wireless access points (APs) is an effective means. However, it significantly increases the cost of network construction for operators. Based on millimeter-wave (mmWave) technology, the 3rd generation partnership project (3GPP) proposed the integrated access and backhaul (IAB) framework to reduce the cost of network construction, which is a promising next generation wireless access solution [3]. In fact, mmWave technology has already been used in the fifth generation (5G) cellular networks thanks to wide available bandwidth. In addition, deploying dense mmWave APs is also helpful to increase both the spectral/energy efficiency of networks and the probability of line-of-sight (LOS) communication.

Due to the densification of mmWave APs, it is cost prohibitive to directly connect them to the core network by fiber or other wired connections. Instead, mmWave backhaul links can be used in dense mmWave multiple access networks, where the same mmWave frequency band is shared by the two types of links (i.e., backhaul and access) in a time-division mode [4]. By using the mmWave backhaul to connect mmWave APs to the micro/macro base stations (MBSs), the existing connection between the core network and the MBSs can be fully exploited to connect APs to core network [5]. In such a scenario, the network efficiency depends on the reasonable wireless resource allocation between the two types of links of each AP. For any AP, its backhaul link and access links are coupled, so wireless resource allocation among them will affect the whole network efficiency [6].

To ensure a high efficiency, jointly optimizing transmission power and access duration is essential. However, due to the interference across backhaul links and access links, it is an arduous task to achieve the optimal resource allocation. If unified transmission duration is adopted by all the APs, the interference between the different types of links can be avoided, but it may not improve the entire network efficiency [7]. References [8], [9] addressed these challenging issues and adopted non-unified access duration allocation and access power adjustment to improve the network efficiency. The constraint on the backhaul data rate in each AP arises the difficulty of finding the optimal solution, so the solution in [8] is not viable in practice due to the high overhead. To overcome this deficiency, reference [9] proposed the resource allocation algorithms with lower complexity by using potential game [10]. However, the existing similar works to those of reference [9] cannot improve the system performance in the face of the scenario with long backhaul links.

Due to the limitations of network construction cost and geographical location, the APs with wired backhaul links account for a very small percentage of all the APs. In reality, the dense mmWave APs are most needed at hotspots and connected to the MBS via wireless backhaul links. Usually, hotspots are discretely distributed and thus form multiple non-continuous clusters in the MBS coverage. So the existence of long backhaul

Manuscript received 12 December 2022; revised 1 July 2023; accepted 20 August 2023. Date of publication 23 August 2023; date of current version 17 January 2024. This work was supported in part by the National Natural Science Foundation of China under Grants 62272484, 61873352, and 61772553. The review of this article was coordinated by Dr. Kai-Ten Feng. *(Corresponding author: Xiaoheng Deng.)*

Jinsong Gui and Xiaoheng Deng are with the School of Electronic Information, Central South University, Changsha 410083, China (e-mail: jsgui2010@csu.edu.cn; dxh@csu.edu.cn).

Long Yin is with the School of Computer Science and Engineering, Central South University, Changsha 410083, China (e-mail: yin_long@csu.edu.cn).

Lin Cai is with the Department of Electrical and Computer Engineering, University of Victoria, Victoria, BC V8P 5C2, Canada (e-mail: cai@ece.uvic.ca).

Digital Object Identifier 10.1109/TVT.2023.3307692

links is inevitable. According to the cluster model described in [11], [12], the distance between the cluster center and the MBS is slightly more than twice the cluster radius. This makes the backhaul capacity of each AP always lower than its access capacity. Because shortening the direct communication distance can improve the transmission capacity, an AP can replace its long backhaul link with a backhaul path consisting of two short links by selecting another AP as its relaying node. However, the combination of relay mode with the share of same mmWave frequency band will complicate the joint access and backhaul resource allocation problem. How to characterize the resulting additional mutual interference relationships will be what we have to focus on.

On the other hand, due to additional interference factors and high energy efficiency optimization requirements, besides access duration allocation, it is necessary to coordinate the transmission power allocation among the access, backhaul and relay sides. Therefore, this makes the problem solution space grow rapidly. It is impossible to directly transplant the game-based schemes similar to those in [9] to quickly find a feasible solution from this huge space. Moreover, in the existing works related to joint backhaul and access resource allocation, the studies aimed at optimizing data rate are relatively less energy-efficient, while the researches aimed at improving energy efficiency do not always ensure that data rate is also optimized. In the video surveillance applications, these two performance metrics are desired by users at the same time. In this article, we address the above challenges and list the main contributions below.

1) We model the joint transmission power adjustment and non-unified backhaul/access transmission duration allocation problem in a relay-assisted wireless backhauling mmWave access network as the optimization problem with the limited backhaul data rate, where the goal is to improve both network sum rate and network energy efficiency.
2) To deal with the formulated problem in a less computationally complex way, we further model the above optimization problem as a Stackelberg game [13] with the feature of sequential decision, where the entire network serves as the leader and all the smart wireless devices serve as the followers.
3) The proposed scheme greatly reduces the solution space when compared with centralized and unified decision-making schemes. In addition, because the leader makes decisions on behalf of all the APs, its solution space is much larger than that of each follower. By adopting the concurrent binary search on the two-dimensional solution space, the leader can accelerate the approximation of optimal solution.
4) In this article, the utility function design for each follower's game decision aims at optimizing its individual access data rate, while that for the leader's game decision aims at optimizing whole network energy efficiency. The simulation results show that such a differentiated design can enhance both network sum rate and network energy efficiency.

The rest of this article is organized as follows. In Section II, we review the relevant works. Then, we describe the system model in Section III, and detail the joint power adjustment and transmission duration allocation scheme in Section IV. Finally, we analyze simulation results in Section V and summarize this article in Section VI.

II. Related Work

In the references related to the subject of this article, most of them aimed at data rate optimization, but a few works were concerned about energy efficiency. In the studies that aimed at data rate optimization, the typical latest works are summarized as follows.

The references [6], [7], [14], [15], [16] focused on the frequency resource reuse (or bandwidth allocation) between backhaul side and access side in a time-division mode to improve data rate. The references [8], [9] studied the joint access and backhaul resource allocation problem for the purpose of enhancing network sum rate by adopting potential game theory to formulate this problem. The reference [17] improved system data rate by designing a dynamic relay probing and decentralized mode selection scheme.

The reference [18] aimed at solving the blockage problem in mmWave backhaul networks and maximizing the number of the flows satisfying their minimum data rate requirements by proposing a relay selection algorithm and a transmission scheduling algorithm. The reference [19] considered the degree of satisfaction of user access capacity under the radio backhaul capacity constraints. The reference [20] investigated how to enhance the weighted data rate through user association, beamforming design, and allotted time between access and backhaul links. The reference [21] described standardized activities for integrating backhaul and access mmWave networks and summarized its pros and cons.

Based on IAB architecture, the reference [22] studied spectrum and power allocation problem, which aims to consider data rate requirements of IAB-based mmWave networks and improve network sum rate. The reference [23] focused on the scenario where unmanned aerial vehicles (UAVs) are deployed not only as APs to provide access links but also as relays to supply backhaul links. The authors theoretically analyzed the optimization problem of network data rate and derived the optimal resource allocation scheme for all the transmission links. The reference [24] determined the most appropriate AP for each access user by considering constraints such as backhaul capacity and link latency. The reference [3] proposed a joint load balance and interference suppression framework to optimize network sum rate. The authors iteratively optimized association of user equipment and allocation of transmission power to facilitate reasonable resource allocation.

Unlike the above works, there are also some typical up-to-date works on energy efficiency optimization. The reference [25] discussed how to enhance energy efficiency of mmWave backhaul links through scheduling optimization and transmission power control. The reference [26] investigated how to enhance energy efficiency of self-backhaul energy harvesting small cells by considering the changes of the energy harvesting rate and the small cells' remaining energy. The reference [27] discussed how

to enhance access links' energy efficiency of self-backhauling small cells through the reasonable power allocation and beamforming design. The references [28], [29] investigated how to address the blocking issue of access links to improve energy efficiency in dense mmWave cellular networks. The reference [28] adopted inband device-to-device (D2D) communication mode to avoid obstacles, while the reference [29] used outband D2D communication mode to achieve the same goal and considered the power adjustment of backhaul links.

Except for the reference [18], the above works did not introduce the relay mode to tackle the backhaul performance bottleneck problem. However, as mentioned above, the reference [18] aimed at solving the backhaul blockage problem, while this article will focus on the performance bottleneck problem caused by overlong backhaul distance. Meanwhile, the reference [18] focused on both maximizing the number of the flows and ensuring their minimum data rate requirements, while this article aims at the improvement of both individual data rate and network energy efficiency. In addition, compared with the mobile smart devices carried by users, massive video acquisition devices in smart cities are relatively static. Therefore, the blocking problem caused by random movement of access terminals is not a primary concern. However, it is of great practical significance to explore the methods that can ensure both data rate and energy efficiency in the video surveillance applications in smart cities, where the APs' coverage area is relatively small, their distribution density is relatively high, and the access terminals are stationary.

III. System Model

A. Network Architecture

We consider an uplink transmission scenario in a relay-assisted self-backhauling dense mmWave multiple access network. The scenario includes one MBS, multiple APs, and many smart IoT devices (SITDs). These SITDs are typically non-mobile smart video camera devices. They can handle the collected video data appropriately, and then send the preliminary processed data to edge (or cloud) servers through nearby APs for detailed analysis. We assume that there are always a large number of the SITDs that request APs to provide access services. Usually, each AP has a limited number of concurrent access links, so its access links are always occupied by incoming requests. The number of concurrent links for each AP depends on the number of its radio frequency (RF) chains.

Unlike the solutions to ensure beam alignment by adjusting beam direction, which is an effective way to deal with terminal mobility, we believe that keeping all the beam azimuths unchanged for each AP is sufficient to meet static SITDs' access demands without complicating the solution. We assume that each RF chain of the same AP uses a non-overlapping beam exclusively, so the RF chains of the same AP can use the same frequency band. Moreover, we suppose that the wireless backhaul/access links reuse the same mmWave bandwidth, so the time-division scheme is used in both types of links.

To facilitate the explanation of the problem without complicating the scenario diagram, we show just one cluster for the macro/micro cell in Fig. 1. In fact, according to the cluster

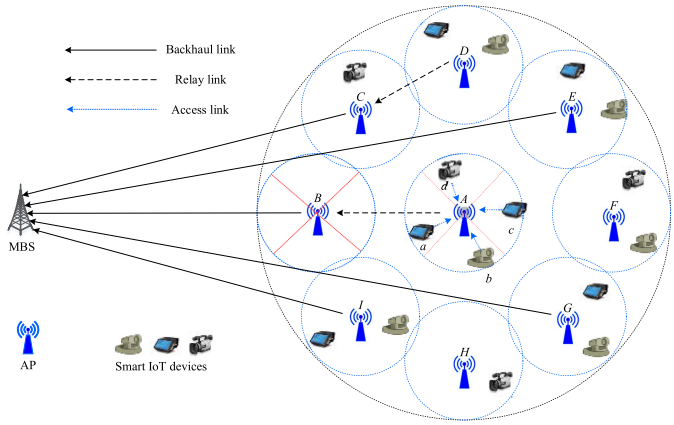

Fig. 1. Relay-assisted self-backhauling dense mmWave multiple access communication scenario.

model described in [11], [12], there are several clusters, where the distance from each cluster center to the MBS is slightly more than twice the cluster radius. As shown in Fig. 1, the mmWave APs are deployed in the cluster based on the description in [11], [12], where a large number of SITDs are randomly distributed in the cluster and the average length of backhaul links of the APs is typically much larger than that of their access links. Moreover, the length of the backhaul links also varies greatly. It is worth noting that not all the APs' backhaul links can be used simultaneously in the scenario in Fig. 1. For example, APs *A*, *B*, and *F* cannot use their own backhaul links simultaneously due to high mutual interference, since their beamwidths towards the MBS overlap. Similarly, APs *C* and *D* (or APs *H* and *I*) cannot use their own backhaul links together. Based on these characteristics, only AP *E* and AP *G* can use their own backhaul links without restriction.

Usually, the MBS will give the APs with more access traffic requirements a higher priority to use their own backhaul links. In this way, more SITDs' access traffic can be routed through it to the core network. Therefore, if all the APs in Fig. 1 have the transmission requirements for backhaul traffic, APs *B*, *C*, *F*, and *H* should be discouraged to use their own backhaul links due their lower traffic load. If the above case occurs, although AP *B* is not allowed to use its backhaul link to send its access traffic, it can forward backhaul traffic for other APs since its backhaul link is shorter and the channel quality is better than others. In order to avoid interfering with the concurrent transmission of other backhaul links, AP *B* can just provide the relay service for AP *A*. If it provides the relay service for AP *F*, it will interfere with the backhaul link of AP *A*. Similarly, AP *C* can just provide the relay service for AP *D*. If it provides the relay service for AP *E*, it will interfere with the backhaul link of AP *D*. In addition, AP *H* cannot provide the relay service for any AP that has the longer backhaul link than that of AP *H*. Otherwise, it would interfere with the backhaul link of AP *I*.

It is beyond the scope of this article that how the MBS schedules all the APs in Fig. 1 to use their respective backhaul links. However, for the historical backhaul traffic of each AP, we can use the exponential moving average operation method in [30] to make statistics, and design a proportional-fairness-based

scheduling policy to determine which APs should be scheduled to use their respective backhaul links simultaneously. Likewise, it is beyond the scope of this article that how an AP schedules the SITDs covered by it to use its access links. However, for the historical access traffic of each SITD, we can use the above method to make statistics, and design a similar scheduling policy to determine which SITDs should be scheduled to use the AP's access links simultaneously. Due to space constraints, this article only focuses on how to optimize both network sum rate and network energy efficiency through the joint access and backhaul resource allocation after the scheduled APs and SITDs are determined.

When an AP (e.g., *A*) selects another AP (e.g., *B*) as its relaying AP, it simply sends its backhaul traffic to the relaying AP. Then, the relaying AP can receive and forward simultaneously as long as its receiving beamwidth does not overlap with its transmission beamwidth. We assume that each AP has at least two mmWave interfaces, so the above conditions are easily satisfied. However, when this pattern is applied to the access and backhaul links at the same AP, some SITDs may be excluded from the scope of access services provided by this AP. For example, SITD *a* within AP *A*'s coverage will not be served by AP *A*, since the receiving beamwidth in AP *A* for SITD *a* overlaps with the backhaul transmission beamwidth of AP *A*. Therefore, as explained in the background above, it makes sense that the access and backhaul links of each AP are used in a time-division mode.

B. Problem Formulation

For the convenience of the description below, a set of APs is denoted by $\wp = \{1, 2, \ldots, S\}$ and a set of SITDs is denoted by $\mho = \{1, 2, \ldots, U\}$. The architectures of mmWave beamformers mainly include analog/digital/hybrid beamforming. The hybrid beamforming is adopted to form a multi-beam system, since it potentially benefits from both of the analog beamforming and digital beamforming structures [31]. For analytical tractability, the mmWave antenna pattern is regarded as a sectored antenna model widely used for wireless resource control researches [32]. In such a sectored antenna model, the gains for all the angles in the main lobe are a constant, while they are a smaller constant in the side lobe. The transmitting and receiving gains at the SITD u and AP s toward each other can be regarded as the normalized beamforming gains, which can be estimated by

$$g^t_{us}\left(\theta^t_{us}, \phi^t_{us}\right) = \begin{cases} \frac{2\pi-(2\pi-\phi^t_{us})\epsilon}{\phi^t_{us}}, & \text{if } |\theta^t_{us}| \le \frac{\phi^t_{us}}{2} \\ \epsilon, & \text{otherwise,} \end{cases}, \quad (1)$$

$$g^r_{us}\left(\theta^r_{us}, \phi^r_{us}\right) = \begin{cases} \frac{2\pi-(2\pi-\phi^r_{us})\epsilon}{\phi^r_{us}}, & \text{if } |\theta^r_{us}| \le \frac{\phi^r_{us}}{2}, \\ \epsilon, & \text{otherwise.} \end{cases} \quad (2)$$

In (1) and (2), g^t_{us} denotes the transmitting gain at access link l_{us} from SITD u to AP s, and g^r_{us} denotes the receiving gain at l_{us}; θ^t_{us} denotes the beam offset angle of l_{us} relative to the boresight direction of the transmitting beam at SITD u, while θ^r_{us} denotes the beam offset angle of l_{us} relative to the boresight direction of the receiving beam at AP s; ϕ^t_{us} denotes the transmitting beam width of SITD u in l_{us}, and ϕ^r_{us} denotes the receiving beam width of AP s in l_{us}; ϵ denotes the gain in the side lobe ($0 \le \epsilon < 1$ and $\epsilon \ll 1$ for narrow beams).

Likewise, we can compute the transmitting beam gain and receiving beam gain at backhaul link l_s from AP s to the MBS, where the transmitting beam gain is denoted by g^t_s and the receiving beam gain is denoted by g^r_s.

The channel gain g^c_{us} at access link l_{us} from SITD u to AP s can be computed by the following formula [33].

$$g^c_{us} = \left|\chi^c_{us}\delta\left(\tau - \tau_{us}\right)\right|^2. \quad (3)$$

In (3), $\delta(\cdot)$ is the Dirac delta function; τ_{us} and χ^c_{us} are the propagation delay and the amplitude of the access link from SITD u to AP s, respectively. τ_{us} is computed by

$$\tau_{us} = \frac{d_{us}}{c}. \quad (4)$$

In (4), d_{us} denotes the distance from SITD u to AP s, and c is the speed of light. Due to the ultra-dense deployment of APs and the small coverage radius of a single AP, it is realistic to suppose that all the access links are in line-of-sight (LOS) state, which can be computed by the following formula [33].

$$\chi^c_{us} = \frac{\lambda}{4\pi d_{us}}. \quad (5)$$

In (5), λ denotes the wavelength and $\lambda = {}^{c}/_{f_c}$, where f_c denotes the carrier frequency.

Likewise, we can estimate the channel gain g^c_s at backhaul link l_s from AP s to the MBS. Usually, the MBS and APs are static and they are deployed with good planning, so it is realistic to suppose that all the backhaul links are in LOS state.

For the two concurrent links l_{xy} and $l_{x`y`}$ which share the same frequency band, the interfered beam gains [31] of l_{xy} resulting from $l_{x`y`}$ are estimated by

$$g^t_{x`y}\left(\theta^t_{x`y}, \phi^t_{xy`}\right) = \begin{cases} \frac{2\pi-\left(2\pi-\phi^t_{x`y`}\right)\epsilon}{\phi^t_{x`y`}}, & \text{if } \left|\theta^t_{x`y}\right| \le \frac{\phi^t_{x`y`}}{2} \\ \epsilon, & \text{otherwise,} \end{cases}, \quad (6)$$

$$g^r_{x`y}\left(\theta^r_{x`y}, \phi^r_{xy}\right) = \begin{cases} \frac{2\pi-\left(2\pi-\phi^r_{xy}\right)\epsilon}{\phi^r_{xy}}, & \text{if } \left|\theta^r_{x`y}\right| \le \frac{\phi^r_{xy}}{2}, \\ \epsilon, & \text{otherwise.} \end{cases} \quad (7)$$

In (6) and (7), $g^t_{x`y}$ denotes the transmitting interference gain at the desired link $l_{xy}$, while $g^r_{x`y}$ denotes the receiving interference gain at l_{xy}; $\theta^t_{x`y}$ denotes the beam offset angle of the interference link $l_{x`y}$ relative to the boresight direction of the transmitting beam at the desired link $l_{x`y`}$, while $\theta^r_{x`y}$ denotes the beam offset angle of $l_{x`y}$ relative to the boresight direction of the receiving beam at l_{xy}; $\phi^t_{x`y`}$ denotes the transmitting beam width of $l_{x`y`}$, while ϕ^r_{xy} denotes the receiving beam width of l_{xy}. Here x, $x`$, $y$, and $y`$ may refer to one of the MBS, APs, and SITDs, respectively.

In this article, we consider discrete power adjustment per beam for both access links and backhaul links. Let p^t_s and p^t_{us} be the transmission power of AP s on the beam directed to the MBS and the transmission power of SITD u on the beam directed to its associated AP s, respectively. The transmission power p^t_s can be chosen from a predetermined finite set P^t_m, which is denoted

by

$$\mathrm{P}_m^t = \left\{ p_m^{t,1} < p_m^{t,2} < \ldots < p_m^{t,K_m} \right\}. \tag{8}$$

In (8), K_m is the cardinality of the set P_m^t. The transmission power p_{us}^t can be chosen from a planned finite set P_{us}^t, which is denoted by

$$\mathrm{P}_{us}^t = \left\{ p_{us}^{t,1} < p_{us}^{t,2} < \ldots < p_{us}^{t,K_{us}} \right\}. \tag{9}$$

In (9), K_{us} is the cardinality of the set P_{us}^t. To dynamically adjust transmission duration in a relay-assisted backhauling dense mmWave access network according to the traffic variations, we use the mmWave frame structure described in [9], which includes downlink (DL) sweeping subframe, uplink (UL) sweeping subframe, and configurable DL/UL subframe (see the reference [9] for details).

We just focus on UL subframe since only uplink transmission scenario is considered in this article. Each subframe consists of a backhaul transmission duration and an access transmission duration, which is divided in a dynamic way. Moreover, each partition has a changeable transmission duration according to channel and traffic level. We adopt the non-unified transmission duration allocation strategy. That is, let each AP choose a personalized transmission duration in each subframe.

Inspired by [9], the access transmission duration sequence of all the APs can be indicated as $\{\alpha_1^a, \alpha_2^a, \ldots, \alpha_s^a, \ldots, \alpha_S^a\}$. Because a scheduling period consists of multiple time slices in access networks, we suppose that S_s time slices are contained in a scheduling period. Thus, for any AP s, its access transmission duration after normalization meets $\alpha_s^a \in \Omega_t$, $\Omega_t = \{\frac{1}{S_s}, \frac{2}{S_s}, \ldots, \frac{S_s-1}{S_s}\}$.

For analytical tractability, $\{\alpha_1^a, \alpha_2^a, \ldots, \alpha_s^a, \ldots, \alpha_S^a\}$ is sorted in an ascending order, and it is relabeled as $\{\hat{\alpha}_1^a < \hat{\alpha}_2^a < \ldots < \hat{\alpha}_s^a < \ldots < \hat{\alpha}_S^a\}$, where $\hat{\alpha}_1^a$ and $\hat{\alpha}_S^a$ are the minimal value and maximal value among the access transmission durations of all the APs, respectively. We use $L = \langle L_1, L_2, \ldots, L_s, \ldots, L_S \rangle$ to represent the index list of all the APs corresponding to the above ordered access transmission duration sequence, where L_s is the index of the s-th AP. Moreover, two auxiliary constants and an empty set are adopted in this article, in which $\hat{\alpha}_0^a = 0$, $\hat{\alpha}_{S+1}^a = 1$, and $\wp_0 = \emptyset$.

The superposition of non-unified transmission duration allocation mode and relay mode makes the interference of access/backhaul links be more unmanageable. For the access link from SITD u to AP s in the duration of $\hat{\alpha}_l^a - \hat{\alpha}_{l-1}^a$ for $1 \le l \le L_s$, it will be interfered by the following types of interference sources: 1) the access links of APs excluding those with indices in list L being smaller than l; 2) the backhaul and relay links of APs with indices in L being smaller than l. The corresponding interferences can be respectively expressed by

$$I_{us}^a = \sum_{s` \in \wp \setminus \wp_l} \sum_{k \in \mho_{s`} \setminus u} p_{ks`}^t \, g_{ks}^t g_{ks}^c g_{ks}^r, \tag{10}$$

$$I_{us}^b = \sum_{s` \in \wp_l} \begin{pmatrix} \left(1 - D_{s`\widehat{s`}}\right) p_{s`}^t g_{s`s}^t g_{s`s}^c g_{s`s}^r \\ + D_{s`\widehat{s`}} \begin{pmatrix} p_{\widehat{s`}}^t g_{\widehat{s`}s}^t g_{\widehat{s`}s}^c g_{\widehat{s`}s}^r \\ + p_{s`\widehat{s`}}^t g_{s`s}^t g_{s`s}^c g_{s`s}^r \end{pmatrix} \end{pmatrix}. \tag{11}$$

In (10) and (11), I_{us}^a denotes the l_{us}'s interference resulting from the access links of APs, while I_{us}^b denotes the l_{us}'s interference resulting from the backhaul and relay links of APs; $\wp_l$ is the set of APs with indices in L being smaller than l; $\mho_{s`}$ denotes the users (i.e., SITDs) set associated with AP $s`$; $D_{s`\widehat{s`}}$ is a binary indicator variable. If no relaying AP is selected for AP $s`$, $D_{s`\widehat{s`}} = 0$. Otherwise, $D_{s`\widehat{s`}} = 1$, and the selected relaying AP is denoted by $\widehat{s`}$.

For the backhaul link from AP s to the MBS in the duration of $\hat{\alpha}_{l+1}^a - \hat{\alpha}_l^a$ for $L_s \le l \le S$, it will be interfered by the following types of interference sources: 1) the access links of APs with indices in L being more than l; 2) the backhaul and relay links of the APs whose indices in L are smaller than l. Therefore, the corresponding interferences can be respectively expressed by

$$I_s^a = \sum_{s` \in \wp \setminus \wp_l} \sum_{k \in \mho_{s`}} p_{ks`}^t \, g_k^t g_k^c g_k^r, \tag{12}$$

$$I_s^b = \sum_{s` \in \wp_l \setminus s} \begin{pmatrix} \left(1 - D_{s`\widehat{s`}}\right) p_{s`}^t g_{s`}^t g_{s`}^c g_{s`}^r \\ + D_{s`\widehat{s`}} \begin{pmatrix} p_{\widehat{s`}}^t g_{\widehat{s`}}^t g_{\widehat{s`}}^c g_{\widehat{s`}}^r \\ + p_{s`\widehat{s`}}^t g_{s`}^t g_{s`}^c g_{s`}^r \end{pmatrix} \end{pmatrix}. \tag{13}$$

In (12) and (13), I_s^a denotes the l_s's interference resulting from the access links of APs, while I_s^b denotes the l_s's interference resulting from the backhaul and relay links of APs.

For the relay link from AP s to AP $\hat{s}$ in the duration of $\hat{\alpha}_{l+1}^a - \hat{\alpha}_l^a$ for $L_s \le l \le S$, it will be interfered by the following types of interference sources: 1) the access links of APs with indices larger than l; 2) the backhaul and relay links of the APs whose indices in L are smaller than l. The corresponding interferences can be respectively expressed by

$$I_{s\hat{s}}^a = \sum_{s` \in \wp \setminus \wp_l} \sum_{k \in \mho_{s`}} p_{ks`}^t \, g_{k\hat{s}}^t g_{k\hat{s}}^c g_{k\hat{s}}^r, \tag{14}$$

$$I_{s\hat{s}}^b = \sum_{s` \in \wp_l \setminus s, \hat{s}} \begin{pmatrix} \left(1 - D_{s`\widehat{s`}}\right) p_{s`}^t g_{s`\hat{s}}^t g_{s`\hat{s}}^c g_{s`\hat{s}}^r \\ + D_{s`\widehat{s`}} \begin{pmatrix} p_{\widehat{s`}}^t g_{\widehat{s`}\hat{s}}^t g_{\widehat{s`}\hat{s}}^c g_{\widehat{s`}\hat{s}}^r \\ + p_{s`\widehat{s`}}^t g_{s`\hat{s}}^t g_{s`\hat{s}}^c g_{s`\hat{s}}^r \end{pmatrix} \end{pmatrix}. \tag{15}$$

In (14) and (15), $I_{s\hat{s}}^a$ denotes the interference from the access links of APs, while $I_{s\hat{s}}^b$ denotes the interference from the backhaul and relay links of APs.

Due to space limitation, the beam gain estimation of each interference link only in formulas (10) and (11) is taken as an example to be illustrated by legend. The gains g_{ks}^t and g_{ks}^r of interference link l_{ks} are estimated by formulas (6) and (7), as illustrated in Fig. 2. Likewise, the gains $g_{s`s}^t$ and $g_{s`s}^r$ of interference link $l_{s`s}$ as well as the gains $g_{\widehat{s`}s}^t$ and $g_{\widehat{s`}s}^r$ of interference link $l_{\widehat{s`}s}$ are also estimated by formulas (6) and (7), as illustrated in Fig. 3. It is worth noting that $s`$ and $s``$ in Fig. 3 belong to the set $\wp_l$ in formula (11).

The signal to interference and noise ratio (SINR) of the access link from SITD u to AP s in the duration of $\hat{\alpha}_l^a - \hat{\alpha}_{l-1}^a$ for $1 \le l \le L_s$ is estimated by

$$SINR_{us}^l = \frac{p_{us}^t g_{us}^t g_{us}^c g_{us}^r}{I_{us}^a + I_{us}^b + WN_0}. \tag{16}$$

In (16), W is mmWave bandwidth reused by all the APs, while N_0 is background noise power spectrum density. Likewise, in

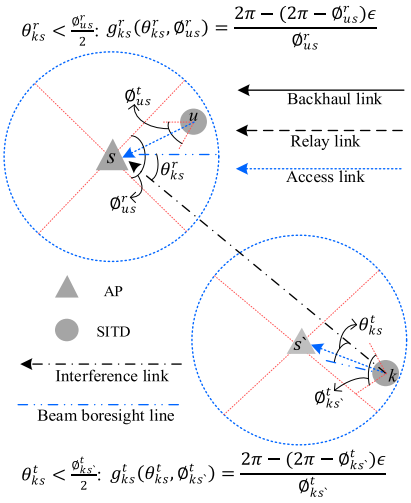

Fig. 2. Access link being interfered by other access links.

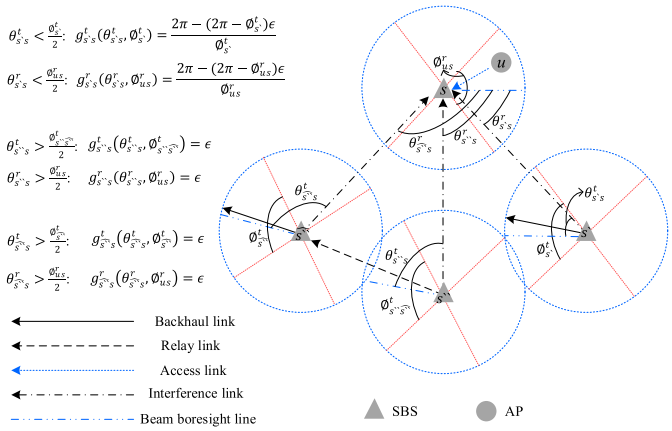

Fig. 3. Access link being interfered by relay links and backhaul links.

duration of $\hat{\alpha}^a_{l+1} - \hat{\alpha}^a_l$ for $L_s \le l \le S$, SINR of backhaul link from AP s to the MBS can be estimated by

$$SINR^l_s = \frac{p^t_s g^t_s g^c_s g^r}{I^a_s + I^b_s + WN_0}. \tag{17}$$

Also, in the duration of $\hat{\alpha}^a_{l+1} - \hat{\alpha}^a_l$ for $L_s \le l \le S$, the SINR of the relay link from AP s to AP $\hat{s}$ that provides the relay service to AP s is estimated by

$$SINR^l_{s\hat{s}} = \frac{p^t_{s\hat{s}} g^t_{s\hat{s}} g^c_{s\hat{s}} g^r_{s\hat{s}}}{I^a_{s\hat{s}} + I^b_{s\hat{s}} + WN_0}. \tag{18}$$

For the u-th SITD of the s-th AP, its data rate T^a_{us} can be given by

$$T^a_{us} = W \sum_{l=1}^{L_s} \left(\hat{\alpha}^a_l - \hat{\alpha}^a_{l-1}\right) \log_2\left(1 + SINR^l_{us}\right). \tag{19}$$

For the s-th AP, its access data rate T^a_s and backhaul data rate T^b_s can be given by

$$T^a_s = W \sum_{u \in \mho_s} \sum_{l=1}^{L_s} \left(\hat{\alpha}^a_l - \hat{\alpha}^a_{l-1}\right) \log_2\left(1 + SINR^l_{us}\right), \tag{20}$$

$$T^b_s = W \sum_{l=L_s}^{S} \left(\hat{\alpha}^a_{l+1} - \hat{\alpha}^a_l\right) \log_2\left(1 + SINR^l_s\right). \tag{21}$$

If s-th AP selects $\hat{s}$-th AP as its relaying AP, its data rate can be expressed by

$$T^b_s = \min\left\{T^b_{s\hat{s}}, T^b_{\hat{s}}\right\}. \tag{22}$$

In (22), $T^b_{\hat{s}}$ is estimated by the formula (21) and $T^b_{s\hat{s}}$ is estimated by

$$T^b_{s\hat{s}} = W \sum_{l=L_s}^{S} \left(\hat{\alpha}^a_{l+1} - \hat{\alpha}^a_l\right) \log_2\left(1 + SINR^l_{s\hat{s}}\right). \tag{23}$$

Based on the application scenario which is concerned in this article, $T^b_{\hat{s}}$ is usually less than $T^b_{s\hat{s}}$. The average energy efficiency of data transmission of entire network is estimated by

$$E_m = \frac{\sum_{s=1}^{S} \min\left\{T^b_s, T^a_s\right\}}{\sum_{s=1}^{S} \left((1-\alpha^a_s)\begin{pmatrix} P_{RF} + (1-D_{s\hat{s}})\, p^t_s \\ +D_{s\hat{s}}\ (p^t_{s\hat{s}} + p^t_{\hat{s}}) \end{pmatrix} + \alpha^a_s \sum_{u \in \mho_s} (P_{RF} + p^t_{us})\right)}. \tag{24}$$

In (24), P_{RF} is the power consumed by an RF chain [34] and $D_{s\hat{s}}$ has the same meaning as $D_{s\hat{s}}$. To improve (or optimize) network energy efficiency, the joint discrete transmission power adjustment and transmission duration allocation optimization problem can be formulated by

$$\begin{cases} \max\limits_{\{\alpha^a_s | s \in \wp\}, \{p^t_s | s \in \wp\}} E_m, \\ \{p^t_{s\hat{s}} | s \in \wp, \hat{s} \in \wp \backslash s\} \\ \text{s.t. } C1:\ T^a_s \le T^b_s,\ \forall s, \\ C2: \alpha^a_s \in \Omega_t,\ \forall s, \\ C3: p^t_s, p^t_{s\hat{s}}, p^t_{\hat{s}} \in \mathrm{P}^t_m,\ \forall s, \hat{s}. \end{cases} \tag{25}$$

In (25), the constraint $C1$ is imposed to guarantee that any AP's access data rate in the current scheduling period cannot be more than its mmWave backhaul data rate; the constraint $C2$ means the available values of the access transmission duration for each AP; the constrain $C3$ offers the available transmission power levels for each AP.

For the u-th SITD of the s-th AP, to improve (or optimize) the data rate of its mmWave access link, the discrete power adjustment problem can be modeled as follows when the s-th AP's transmission duration α^a_s is given.

$$\begin{cases} \max\limits_{p^t_{us} \in \mathrm{P}^t_{us}} T^a_{us}, \\ \text{s.t. } C1;\ C4: p^t_{us} \in \mathrm{P}^t_{us}, \forall s. \end{cases} \tag{26}$$

In (26), the constraint $C1$ is same as that of (25), and the constraint $C4$ provides the available transmission power levels for each end user (i.e., SITD).

IV. Joint Power Adjustment and Transmission Duration Allocayion

A. The Reasons for Choosing Stackelberg Game

We see that the problems (25) and (26) are combinatorial and non-convex. The non-convexity mainly comes from constraint $C1$, while the combinatorial property results from constraints $C2$, $C3$ and $C4$. To solve problem in a less computationally complex way, the potential game is adopted to model the optimization problem described in [9], but it hardly characterizes the correlation between problems (25) and (26). This deficiency can be compensated by using a Stackelberg game, which is a sequential game composed of a leader and multiple followers. Therefore, we formulate the two interrelated optimization problems as a Stackelberg game, in which the network (including the MBS and all the APs) acts as the leader and each SITD serves as the follower. The leader expects to obtain the solution for problem (25), while each follower wants to obtain the solution for problem (26). They compete with each other for the portion of time slices during a scheduling period composed of the fixed number of time slices, where the leader makes a decision first (i.e., it specifies an access transmission duration and a transmission power for each AP) after considering the followers' behaviors and the followers make decisions subsequently.

For a follower (e.g., the u-th SITD of the s-th AP), when observing the access transmission duration of the s-th AP determined by the leader, it selects a transmission power from the set P_{us}^{t} to approach the optimum solution for problem (26). Since a follower's action to solve problem (26) affects the other followers' decision, this interaction problem is formulated by a potential game. Usually, on the basis of the assumption that the leader gives a decision, we solve a potential game Nash equilibrium (NE) for all the followers. Then, by adopting a backward induction method, we can derive the leader's decision-making expression. However, when designing algorithms to solve the above problems, the leader may first initialize the transmission power and transmission duration for each AP to a pair of conservative values. Following the leader, each SITD acting as a follower determines its transmission power according to its own utility function. After observing the followers' decision results, the leader will make decisions based on its own utility function. This process repeats until the game reaches a SNE. In the following text, we will discuss the corresponding details.

B. SITD-Level Game Analysis and Solution

As a follower, each SITD is self-interested and its goal is to make as much profit as possible, where the profit is its access link data rate. Each SITD adopts its transmission power as its action strategic variable to improve its personalized profit. For the u-th SITD of the s-th AP, the data rate of its access link l_{us} relies on not only its choosing power p_{us}^{t} from the set P_{us}^{t} but also the other SITDs' choosing powers. The main reason is that all the SITDs reuse the same mmWave bandwidth and thus they interfere with each other. The transmission power selection decision problem can be formulated by a potential game, where the set of game players is $\mho = \{1, 2, \ldots, U\}$ and the set of strategy sets is $\{\mathrm{P}_{us}^{t} | s \in \wp, u \in \mho_s\}$. For a game player (e.g., SITD u, $u \in \mho_s$) in the coverage of an AP (e.g., $s \in \wp$), its strategy set is P_{us}^{t}, and the corresponding utility function is formulated by

$$\mu_{us} = (1-\varphi)\begin{pmatrix} \sum_{s=1}^{S} T_s^a + \\ e_t \sum_{s=1}^{S} \Phi\left(T_s^b, T_s^a\right) \end{pmatrix} + \varphi \begin{pmatrix} T_{us}^a + \\ e_s \Phi\left(T_s^b, T_s^a\right) \end{pmatrix}. \tag{27}$$

In (27), e_s and e_t denote the non-negative penalty scalar and their unit is "*bps/Watt*"; $\Phi(x, y)$ denotes the penalty function discussed in [9], [34], which satisfies that $\Phi(x, y) = -1$ if $x < y$, and $\Phi(x, y) = 0$ if $x \geq y$; φ denotes a weight coefficient and $0 < \varphi < 1$, which refers specifically to the ratio of the game player u's actual benefit to its utility value. The first term in (27) corresponds to the part of the total utility resulting from the sum data rate of all the game players' access links, where the first term in parentheses is the sum data rate of all the game players' access links, while the second term in parentheses represents all the APs' backhaul constraints. These backhaul constraints imply that a SITD will be punished if it chooses a strategy violating constraint $C1$. The second term in (27) corresponds to the part of the total utility resulting from the data rate of the player u's access link, where the first term in parentheses is the data rate of the player u's access link, while the second term in parentheses represents AP s's backhaul constraint. This backhaul constraint implies that the game player u should be punished if it chooses a strategy violating constraint $C1$.

According to the definition in [10], the established game model can easily be proved to conform to the characteristics of potential game, where $\sum_{s=1}^{S} \sum_{u \in \mho_s} \mu_{us}$ is its potential function. There are several nice properties for the potential game, where there is at least one pure strategy NE. If there does not exist constraint $C1$, each NE is a solution for the established potential game model. Because of the constraint $C1$, it is unclear whether each NE can meet this constraint or not, though there may be one viable pure strategy NE. To facilitate the discussion below, the maximum values of e_s and e_t are denoted by $e_s^{\max}$ and $e_t^{\max}$ respectively, where $e_s^{\max} = \max_{u \in \mho_s} T_{us}^a$ and $e_t^{\max} = \max \sum_{s=1}^{S} T_s^a$.

If dense mmWave access networks use the scheduling scheme with the same transmission time interval as that of low frequency networks, wider subcarrier spacing will generate more time slices in a scheduling period of dense mmWave access networks. In order to give the proof for the viable NE existence of the established potential game model, we use the assumption in [9]: each scheduling period includes sufficient time slices in a mmWave band because its subcarrier spacing is much wider than that in a low frequency band. According to this assumption, it is not difficult to deduce that there must be some viable action strategies for the game player who can satisfy constraints C1 and C4.

The potential game NE gives the set of transmission powers (e.g., (A_u^*, A_{-u}^*)) such that any SITD cannot improve its

utility by updating its current transmission power (i.e., A_u^*) to a different transmission power (e.g., A_u), given the transmission powers (i.e., A_{-u}^*) offered by the other SITDs. That is, if $\mu_{us}(A_u^*,\ A_{-u}^*) \geq \mu_{us}(A_u, A_{-u}^*)$, $(A_u^*,\ A_{-u}^*)$ is a pure strategy NE of the potential game model established in this subsection. The following Lemma 1 offers the analysis for the feasibility of pure strategy NE of the established potential game model.

Lemma 1: The pure strategy NE of the established potential game model must be viable, if $e_s \geq e_s^{\max}$ and $e_t \geq e_t^{\max}$ as well as each scheduling period contains plenty of time slices and the variations of access transmission durations of all the APs have no effect on one another under the constraint C1.

Proof: Let the action profile $(A_1^*, A_2^*, \ldots, A_u^*, \ldots, A_U^*)$ be a pure strategy NE of the established potential game model, which is assumed to violate the constraint C1. Then, there must exist at least an AP whose access data rate is more than its backhaul data rate. Without loss of generality, this AP is denoted by the game player $\mu` \in \{1, 2, \ldots, U\}$. Since it is assumed that each scheduling period includes plenty of time slices, the game player $\mu`$ can select another action $A_{u`}^{`}$ with a shorter access transmission duration to make its backhaul data rate be more than its access data rate. Therefore, if the variations of access transmission durations of all the APs do not affect one another with respect to constraint C1, we have

$$\begin{aligned}
&\mu_{us}\left(A_{u`}^*,\ A_{-u`}^*\right) - \mu_{us}\ \left(A_{u`}^{`},\ A_{-u`}^*\right)\\
&= \varphi\{\left(T_{us}^a\left(A_{u`}^*,\ A_{-u`}^*\right) - T_{us}^a\left(A_{u`}^{`},\ A_{-u`}^*\right)\right)\\
&\quad + e_s(\Phi\left(T_s^b\left(A_{u`}^*,\ A_{-u`}^*\right), T_s^a\left(A_{u`}^*,\ A_{-u`}^*\right)\right)\\
&\quad - \Phi\left(T_s^b\left(A_{u`}^{`},\ A_{-u`}^*\right), T_s^a\left(A_{u`}^{`},\ A_{-u`}^*\right)\right))\}\\
&\quad + (1-\varphi)\left\{\sum_{s=1}^{S}\begin{pmatrix} T_s^a\left(A_{u`}^*,\ A_{-u`}^*\right) - \\ T_s^a\left(A_{u`}^{`},\ A_{-u`}^*\right)\end{pmatrix}\right.\\
&\quad \left. + e_t\begin{pmatrix}\sum_{s=1}^{S}\Phi\left(T_s^b\left(A_{u`}^*,\ A_{-u`}^*\right), T_s^a\left(A_{u`}^*,\ A_{-u`}^*\right)\right) - \\ \sum_{s=1}^{S}\Phi\left(T_s^b\left(A_{u`}^{`},\ A_{-u`}^*\right), T_s^a\left(A_{u`}^{`},\ A_{-u`}^*\right)\right)\end{pmatrix}\right\}\\
&= \varphi\left\{\left(T_{us}^a\left(A_{u`}^*,\ A_{-u`}^*\right) - T_{us}^a\left(A_{u`}^{`},\ A_{-u`}^*\right)\right) - e_s\right\}\\
&\quad + (1-\varphi)\left\{\sum_{s=1}^{S}\begin{pmatrix} T_s^a\left(A_{u`}^*,\ A_{-u`}^*\right) - \\ T_s^a\left(A_{u`}^{`},\ A_{-u`}^*\right)\end{pmatrix} - e_t\right\} < 0. \quad (28)
\end{aligned}$$

Obviously, (28) contradicts the assumption that $(A_1^*, A_2^*, \ldots, A_u^*, \ldots, A_U^*)$ is a pure strategy NE of the established potential game model. Thus, the pure strategy NE of the established potential game model must be viable if the conditions of this Lemma are satisfied. The proof is completed.

Lemma 1 manifests that the viable solution to the formulated potential game model is guaranteed under certain conditions. That is, not all the pure strategy NE of potential game are viable if the following assumption is not satisfied: the variations of access transmission durations of all the APs have no impact on one another with respect to constraint C1. Next, we discuss the existence of the viable pure strategy NE of the formulated potential game model in Lemma 2.

Lemma 2: The established potential game model has at least one viable pure strategy NE and the optimal solution of the problem (26) forms a pure strategy NE of the established potential game model, if $e_s \geq e_s^{\max}$ and $e_t \geq e_t^{\max}$ as well as each scheduling period contains plenty of time slices.

Proof: Let $F = \sum_{s=1}^{S}\sum_{u\in\mho_s}\mu_{us}$ and $(A_1^*, \ldots, A_u^*, \ldots, A_U^*)$ be the best action profile of F. If the conditions of this Lemma are met, $F(A_1^*, \ldots, A_u^*, \ldots, A_U^*) > 0$. However, if $(A_1^*, \ldots, A_u^*, \ldots, A_U^*)$ is not viable, we have $F(A_1^*, \ldots, A_u^*, \ldots, A_U^*) < 0$, which contradicts the above inequality. Therefore, when $e_s \geq e_s^{\max}$ and $e_t \geq e_t^{\max}$ hold, $(A_1^*, \ldots, A_u^*, \ldots, A_U^*)$ must be viable, and we have

$$\begin{aligned}
&F\ (A_1^*, \ldots, A_u^*, \ldots, A_U^*)\\
&= \sum_{s=1}^{S}\sum_{u\in\mho_s}\begin{pmatrix}\varphi T_{us}^a\left(A_1^*, \ldots, A_u^*, \ldots, A_U^*\right)\\ +(1-\varphi)\sum_{s=1}^{S}T_s^a\left(A_1^*, \ldots, A_u^*, \ldots, A_U^*\right)\end{pmatrix}.
\end{aligned} \quad (29)$$

where $T_s^a\ (A_1^*, \ldots, A_u^*, \ldots, A_U^*) = \sum_{u\in\mho_s} T_{us}^a(A_1^*, \ldots, A_u^*, \ldots, A_U^*)$. For any action profile $(A_1, \ldots, A_u, \ldots, A_U)$, if the conditions of this lemma are met, $F(A_1^*, \ldots, A_u^*, \ldots, A_U^*) \geq F(A_1, \ldots, A_u, \ldots, A_U)$, and then we have

$$\begin{aligned}
&\sum_{s=1}^{S}\sum_{u\in\mho_s}\begin{pmatrix}\varphi T_{us}^a\left(A_1^*, \ldots, A_u^*, \ldots, A_U^*\right) +\\ (1-\varphi)\sum_{s=1}^{S}T_s^a\left(A_1^*, \ldots, A_u^*, \ldots, A_U^*\right)\end{pmatrix} \geq\\
&\sum_{s=1}^{S}\sum_{u\in\mho_s}\begin{pmatrix}\varphi T_{us}^a\left(A_1, \ldots, A_u, \ldots, A_U\right)\\ +(1-\varphi)\sum_{s=1}^{S}T_s^a\left(A_1, \ldots, A_u, \ldots, A_U\right)\end{pmatrix}.
\end{aligned} \quad (30)$$

where $T_s^a\ (A_1, \ldots, A_u, \ldots, A_U) = \sum_{u\in\mho_s} T_{us}^a(A_1, \ldots, A_u, \ldots, A_U)$. Therefore, $(A_1^*, \ldots, A_u^*, \ldots, A_U^*)$ is a viable solution to the problem (26).

Then, there does not exist any action profile $(A_1, \ldots, A_u, \ldots, A_U)$, $\forall A_u \in \mathrm{P}_{us}^t$, such that $T_{us}^a(A_1, \ldots, A_u, \ldots, A_U)$ is more than $T_{us}^a(A_1^*, \ldots, A_u^*, \ldots, A_U^*)$ according to the potential game properties.

Moreover, if A_u, for $u \in \mho_s \subset \mho$, is an alternate action of game player u, where $A_u \in \mathrm{P}_{us}^t$ and $A_u \neq A_u^*$, we then have $\mu_{us}(A_u, A_{-u}^*) \leq \mu_{us}(A_u^*, A_{-u}^*)$. In other words, any game player cannot unilaterally change its action to enhance its utility. Thus, on the basis of the definition of NE, $(A_1^*, \ldots, A_u^*, \ldots, A_U^*)$ is a pure strategy NE of the established potential game model, and thus it is also the viable solution of the problem (26). So $(A_1^*, \ldots, A_u^*, \ldots, A_U^*)$ is a pure strategy NE of the established potential game model, which concludes the proof.

Based on the best response dynamic, we present a potential game decision algorithm, which is described in Algorithm 1. It is worth noting that, because not all the NEs of the established potential game model are viable, Algorithm 1 need to start with a viable strategy profile to guarantee that it finally converges to a viable pure strategy NE. Thus, in Algorithm 1, the initial access transmission duration for any AP (e.g., s) is the minimum value in its available access transmission duration set, which guarantees that any initial action strategy is viable under the above assumption. Based on the similar proof described in [35], we discuss the convergence performance of the presented

Algorithm 1 in Theorem 1. To facilitate the proof of Theorem 1, we firstly need to prove the following Lemma 3.

Lemma 3: The utility function $\mu_{us}(A_u^t)$ is either concave or non-decreasing in terms of A_u^t on the interval [0, $p_{us}^{\max}$], where $p_{us}^{\max}$ is the maximum power of each SITD.

Proof: Because $\frac{\partial^2 T_{us}^a(A_u^t)}{\partial (A_u^t)^2} < 0$, $T_{us}^a(A_u^t)$ is a concave function with respect to A_u^t on the interval [0,∞). Let $\frac{\partial T_{us}^a(A_u^t)}{\partial A_u^t} = 0$, and then A_u^{t*} corresponding to the maximum function value can be solved in theory. If $A_u^{t*} \geq p_{us}^{\max}$, $T_{us}^a(A_u^t)$ is non-decreasing with respect to p_{us}^t on the interval [0, $p_{us}^{\max}$]. Otherwise, it is a concave function on the same interva. Because T_s^a is the sum function in terms of $T_{us}^a(A_u^t)$, it has the same properties as $T_{us}^a(A_u^t)$. Since $\mu_{us}(A_u^t)$ is the sum function in terms of $T_{us}^a(A_u^t), T_s^a$, and $\Phi(T_s^b, T_s^a)$, we discuss the effect of $\Phi(T_s^b, T_s^a)$ on the properties of $\mu_{us}(A_u^t)$. In view of the piecewise nature of $\Phi(T_s^b, T_s^a)$, it has two types of piecewise values (i.e., 0 and -1). When the case of $T_s^b < T_s^a$ does not occur on the interval [0, $p_{us}^{\max}$], it does not affect the properties of $\mu_{us}(A_u^t)$ on the same interval since $\Phi\ (T_s^b, T_s^a) = 0$. So $\mu_{us}(A_u^t)$ has the same properties as $T_{us}^a(A_u^t)$. If the case of $T_s^b < T_s^a$ occurs on the interval [0, $p_{us}^{\max}$], the function value interval of $\mu_{us}(A_u^t)$ on the interval [0, $p_{us}^{\max}$] is split into two or more ranges, where the utility function in each range is either concave or non-decreasing. The proof is completed.

Theorem 1: Algorithm 1 converges to a viable pure strategy NE of the established potential game model in the finite steps from any initial viable action strategy profile, if $e_s \geq e_s^{\max}$ and $e_t \geq e_t^{\max}$ as well as each scheduling period contains plenty of time slices.

Proof: Based on Lemma 3, we know that, the range of viable action strategy profiles falls within the interval [0, A_u^{t*}]. When $A_u^{t*} \geq p_{us}^{\max}$, the range is limited in [0, $p_{us}^{\max}$] if the case of $T_s^b < T_s^a$ does not occur on the interval [0, $p_{us}^{\max}$], otherwise, it is limited in [0, A_u^{t**}] and $A_u^{t**} < p_{us}^{\max}$. Here, A_u^{t**} is the maximum power for which the condition (i.e., $T_s^b \geq T_s^a$) holds. Similarly, when $A_u^{t*} < p_{us}^{\max}$, the range is limited in [0, A_u^{t*}] if the case of $T_s^b < T_s^a$ does not occurs on the same interval, otherwise it is limited in [0, A_u^{t**}] and $A_u^{t**} < A_u^{t*}$. Starting from any action profile that is initially viable, based on best response, we have

$$\mu_{us}\left(A_u^{t+1}, A_{-u}^t\right) > \mu_{us}\left(A_u^t, A_{-u}^t\right),\ \forall u \in \mho_s \subset \mho, \quad (31)$$

which points out that the utilities of all the players strictly increases with each iteration. Let $F = \sum_{s=1}^{S} \sum_{u \in \mho_s} \mu_{us}$ and F^* be the maximum value of F, we have $F^* < \infty$ due to the finite number of each player's action strategies and the finite number of players. Furthermore, the established potential game model is a potential game with potential function F, then we have

$$\mu_{us}\left(A_u^{t+1}, A_{-u}^t\right) - \mu_{us}\left(A_u^t, A_{-u}^t\right) > 0 \Leftrightarrow F\left(A_u^{t+1}, A_{-u}^t\right) - F\left(A_u^t, A_{-u}^t\right) > 0,\ \forall u \in \mho_s \subset \mho. \quad (32)$$

According to (31) and (32), we can come to a conclusion that each change of a player's action strategy at each iteration will lead to a strict increasing quantity of F. Since $F^* < \infty$, there must be t^* to meet $0 \leq t^* < \infty$, which has $F\left(A_u^{t^*}, A_{-u}^{t^*}\right) = F^*$ when t^* is big enough. That is, the strict increasing process of the presented algorithm must converge in the finite steps. The proof is completed.

Algorithm 1: Discrete Power Adjustment by Best Response.

Run at each SITD (e.g., $u \in \mho_s$)
Input: the power set P_{us}^t and the access transmission duration α_s^a
Output: the desired power p_{us}^t selected from the set P_{us}^t

1: Initialize $A`_u$ to the minimum power in P_{us}^t and send it to the MBS
2: **If** receive A_{-u} from the MBS **then**
3: $\mu_{us}^b \leftarrow \mu_{us}(A`_u, A_{-u})$
4: $A_u = \text{argmax}_{A``_u \in \mathrm{P}_{us}^t} \mu_{us}(A``_u, A_{-u})$
5: $\mu_{us}^a \leftarrow \mu_{us}(A_u, A_{-u})$
6: **If** $\mu_{us}^a > \mu_{us}^b$ **then**
7: Send A_u to the MBS
8: $A`_u \leftarrow A_u$ and go to 2
9: **Else**
10: Send $A`_u$ to the MBS
11: **End if**
12: **End if**
13: **If** receive "end" from the MBS **then** return **End if**
14: Go to 2

Run at the MBS
Input: null
Output: $A_1 \times \ldots \times A_u \times \ldots \times A_U$

1: Initialize the set $\mathbb{N}$ to $\emptyset$ (i.e., an empty set)
2: **If** receive the new power A_u from any SITD u **then**
3: Update $(A_u, A_{-u}) = A_1 \times \ldots \times A_u \times \ldots \times A_U$
4: **Else if** receive the old power $A`_u$ **then**
5: $\mathbb{N} \leftarrow \mathbb{N} \cup \{u\}$
6: **End if**
7: **If** $|\mathbb{N}| < U$ **then**
8: Send (A_u, A_{-u}) to all the SITDs
9: **Else**
10: Send the packet including "end" to all the SITDs
11: **End if**

Although the transmission powers have not yet been finalized for all the players, the other parameters used to estimate the utility of each player (e.g., u) according to the formula (27) can be available in advance (e.g., after SITD u is associated with the AP s). Therefore, as long as player u can get the transmission powers updated by the other players in time, its utility can be updated in time according to the formula (27). The information exchange of this kind of transmission powers can be accomplished in a broadcasting mode among the players. In addition, a central node can be used for collection and distribution of this kind of transmission powers, which is adopted in Algorithm 1 since this exchange mode has the lower overhead.

In Algorithm 1, when player u needs to calculate its utility, it sends a request of collecting the other players' transmission powers to the MBS through its sub-6 GHz channel, where player u's behavior of reporting the selected power to the MBS is considered as such a request. Since the other players act like this player after the game process is started, the MBS will gather the latest transmission powers of all the players and thus it broadcasts this information to all the players through a common sub-6 GHz channel. Starting from the preliminary viable strategy profile, based on best response dynamic, all the players' utilities are not decreasing in the range of viable action strategy profiles after each iteration. In addition, because the number of each player's strategies and the number of players is not infinite, Algorithm 1 must converge in the finite steps. However, in line 4 of Algorithm 1, player u should go through all of its strategies to determine the best one so far. Therefore, a binary search method can be considered to accelerate this traversal process. Since the function value interval of $\mu_{us}(A_u^t)$ on the interval [0, $p_{us}^{\max}$] may be split into two or more ranges, a binary search method cannot be directly used to find the approximate optimization solution of $\mu_{us}(A_u^t)$. Therefore, we simplify the formula (27) as the following function.

$$\hat{\mu}_{us} = (1-\varphi)\sum_{s=1}^{S} T_s^a + \varphi T_{us}^a. \tag{33}$$

Obviously, the function $\hat{\mu}_{us}(A_u^t)$ is concave or non-decreasing in terms of A_u^t on the interval [0, $p_{us}^{\max}$]. Therefore, a binary search method cannot be directly used to find the approximate optimization solution of $\hat{\mu}_{us}(A_u^t)$. If this approximate optimization solution does not satisfy the constraint $C1$, the corresponding transmission power should be gradually reduced until the constraint $C1$ is satisfied.

C. MBS-Level Game Analysis and Solution

We have a coupled problem related to backhaul link and multiple access links of each AP. The transmission duration and transmission power adopted by each AP will affect the power level of each access terminal, and vice versa. Therefore, we model the MBS's utility function as follows.

$$\mu_m = E_m + e_m \sum_{s=1}^{S} \Phi\left(T_s^b, T_s^a\right). \tag{34}$$

In (34), e_m is the non-negative penalty scalar and the unit is "*bps/Watt*". It is worth mentioning that the utility function given by (34) is for the entire network. The first term in (34) represents the average energy efficiency of the entire network, and the second term corresponds to the backhaul capacity constraints for all the APs. In other words, if there is any AP that chooses an action strategy violating constraint $C1$, the utility of the entire network will drop.

It is noted that, if $e_m > \max(E_m)$ and there are some viable strategies for the MBS meeting the constraints $C1 \sim C3$, the problem (25) has the same optimal solution as the game model with the utility function (34). Based on these conditions, the strategy of any AP that violates the constraint $C1$ will make μ_m be less than 0, which means the strategy profiles that cannot meet the constraint $C1$ cannot be the optimal solution to the problem (25). To optimize the problem (25), the MBS must determine a pair of strategy sets $\{B_1, B_2, \ldots, B_s, \ldots, B_S\}$ and $\{\alpha_1^a, \alpha_2^a, \ldots, \alpha_s^a, \ldots, \alpha_S^a\}$, where B_1, B_2, ..., B_s, ..., $B_S \in \mathrm{P}_m^t$.

According to the definition given in [10], the problem (25) can indeed be modeled as a potential game with μ_m serving as the potential function. For convenience, the MBS should make game decisions for all the players (i.e., APs) to determine their strategies based on best response dynamic. To avoid being limited to a local point of convergence, the MBS randomly initializes the order in which it makes a decision for each AP in each leader game stage. To accelerate the convergence speed, a binary search method is adopted in both the transmission power dimension and transmission duration dimension by taking advantage of the order of the values in the two dimensions.

Given the backward induction to solve the established Stackelberg game model, we propose an iterative method (i.e., Algorithm 2) to obtain the SNE. In Algorithm 2, each AP's initial access transmission duration is the minimum value in its available access transmission duration set, which means each AP's initial backhaul transmission duration is the maximum value since each scheduling period is fixed. Also, each AP's initial transmission power is the maximum value in its available transmission power set. Therefore, these initial action strategy profiles are viable under the above assumption. Based on the similar proof described in [35], we describe the convergence performance of Algorithm 2 in the following Theorem 2. To facilitate the proof of Theorem 2, we firstly need to prove the following Lemma 4 and Lemma 5. For the sake of description, we rewrite the formula (24) as follows.

$$\begin{cases} E_m\ (B_s^t, \alpha_s^t) = \frac{f(B_s^t, \alpha_s^t)}{h(B_s^t, \alpha_s^t)} \\ f\ (B_s^t, \alpha_s^t) = \sum_{s=1}^{S} \min\left\{T_s^b, T_s^a\right\} \\ h\ (B_s^t, \alpha_s^t) = \sum_{s=1}^{S} \left(\begin{array}{c} (1-\alpha_s^t)\left(\begin{array}{c} P_{RF} + (1-D_{s\hat{s}})\, B_s^t \\ +D_{s\hat{s}}\ (B_s^t + B_{\hat{s}}^t) \end{array} \right) \\ +\alpha_s^t \sum_{u \in \mho_s} (P_{RF} + A_u^t) \end{array} \right) \end{cases}. \tag{35}$$

Lemma 4: The utility function $\mu_m(B_s^t, \alpha_s^t)$ is decreasing in terms of B_s^t on the interval (0, $p_m^{\max}$] when α_s^t is fixed, where $p_m^{\max}$ is the maximum power of each AP.

Proof: When α_s^t is a fixed value, $h(B_s^t, \alpha_s^t)$ is a linearly increasing function in terms of B_s^t on the interval [0, $p_m^{\max}$]. Similarly, if α_s^t is fixed and $T_s^b < T_s^a$, $f(B_s^t, \alpha_s^t)$ is a linearly increasing function in terms of B_s^t on the interval [0, $p_m^{\max}$], otherwise it is equal to a constant value. Obviously, the condition $T_s^b \geq T_s^a$ is what we want, which makes $E_m(B_s^t, \alpha_s^t)$ be a decreasing function in terms of B_s^t on the interval [0, $p_m^{\max}$] due to $\frac{\partial E_m(B_s^t, \alpha_s^t)}{\partial B_s^t} < 0$. Although $\mu_m(B_s^t, \alpha_s^t)$ is the sum function in terms of $E_m(B_s^t, \alpha_s^t)$ and $\Phi(T_s^b, T_s^a)$, we are only interested in the case of $T_s^b \geq T_s^a$. In this case, due to $\Phi\ (T_s^b, T_s^a) = 0$,

$\mu_m(B_s^t, \alpha_s^t)$ has the same properties as $E_m(B_s^t, \alpha_s^t)$. The proof is completed.

Lemma 5: The utility function $\mu_m(B_s^t, \alpha_s^t)$ is concave in terms of α_s^t on the specified interval when B_s^t is fixed.

Proof: When B_s^t is a fixed value, we have

$$\frac{\partial^2 E_m\left(B_s^t, \alpha_s^t\right)}{\partial\left(\alpha_s^t\right)^2} = \begin{pmatrix} \frac{1}{h(B_s^t,\alpha_s^t)} \frac{\partial^2 f(B_s^t,\alpha_s^t)}{\partial(\alpha_s^t)^2} - \\ \frac{f(B_s^t,\alpha_s^t)}{(h(B_s^t,\alpha_s^t))^2} \frac{\partial^2 h(B_s^t,\alpha_s^t)}{\partial(\alpha_s^t)^2} - \\ \frac{2}{(h(B_s^t,\alpha_s^t))^2} \frac{\partial f(B_s^t,\alpha_s^t)}{\partial \alpha_s^t} \frac{\partial h(B_s^t,\alpha_s^t)}{\partial \alpha_s^t} + \\ \frac{2 f(B_s^t,\alpha_s^t)}{(h(B_s^t,\alpha_s^t))^3} \left(\frac{\partial h(B_s^t,\alpha_s^t)}{\alpha_s^t}\right)^2 \end{pmatrix} \tag{36}$$

In (36), $\frac{\partial^2 h(B_s^t,\alpha_s^t)}{\partial(\alpha_s^t)^2} = 0$ since $h(B_s^t, \alpha_s^t)$ is a linear function. Similarly, $\frac{\partial^2 f(B_s^t,\alpha_s^t)}{\partial(\alpha_s^t)^2} < 0$ since $f(B_s^t, \alpha_s^t)$ is a concave function in terms of α_s^t. Let $\frac{\partial f(B_s^t,\alpha_s^t)}{\partial \alpha_s^t} = 0$, and then we solve it to get α_s^{t*}. If $\alpha_s^{t*} > 1$, $f(B_s^t, \alpha_s^t)$ is an increasing function in terms of α_s^t on the interval (0, 1), otherwise it is an increasing function in terms of α_s^t on the interval (0, α_s^{t*}]. So $\frac{\partial f(B_s^t,\alpha_s^t)}{\partial \alpha_s^t} > 0$ on the corresponding interval. In addition, $\sum_{u\in\mho_s}(P_{RF} + A_u^t)$ is usually more than $P_{RF} + (1 - D_{s\hat{s}})B_s^t + D_{s\hat{s}}\ (B_s^t + B_{\hat{s}}^t)$ if $|\mho_s|$ is large enough. So $h(B_s^t, \alpha_s^t)$ is a linear increasing function in terms of α_s^t and thus $\frac{\partial h(B_s^t,\alpha_s^t)}{\partial \alpha_s^t}$ is more than 0. Moreover, when $|\mho_s|$ is large enough, the value of $h(B_s^t, \alpha_s^t)$ is also large enough. Based on the above, $\frac{\partial^2 E_m(B_s^t,\alpha_s^t)}{\partial(\alpha_s^t)^2}$ is less than 0, which shows that the lemma holds.

According to the reference [36], the bivariate optimization problem of the utility function $\mu_m(B_s^t, \alpha_s^t)$ can be decomposed into the two univariate optimization problems. Based on Lemma 4 and Lemma 5, a binary search method can be used to find the suboptimal values B_s^{t*} and α_s^{t*}.

Theorem 2: Algorithm 2 converges to a viable strategy SNE of the established Stackelberg game model in the finite steps from any initial viable action strategy profiles, if $e_m > \max(E_m)$ as well as each scheduling period contains plenty of time slices.

Proof: Based on Lemma 4, we know that, the range of viable power strategy profiles is denoted by $[B_s^{t*}, p_m^{\max}]$, where B_s^{t*} is the approximate minimum power for which the condition (i.e., $T_s^b \geq T_s^a$) holds. Similarly, based on Lemma 5, we know that, the range of viable access duration strategy profiles is denoted by (0, α_s^{t*}]. Starting from any action profile that is initially viable, based on best response, we have

$$\begin{aligned} &\mu_m\left(B_s^{t+1}, B_{-s}^t, \alpha_s^{t+1}, \alpha_{-s}^t\right) \\ &\quad > \mu_m\left(B_s^t, B_{-s}^t, \alpha_s^t, \alpha_{-s}^t\right), \forall\, s \in \wp, \end{aligned} \tag{37}$$

which points out that the utilities of all the players strictly increases with each iteration, where power is reduced and access duration is increased until each player's utility no longer increases. Let $\mu_m^s = \mu_m$ and μ_m^* be the maximum value of μ_m, we have $\mu_m^* < \infty$ due to the finite number of each player's action strategies and the finite number of players. Furthermore, the established potential game model is a potential game with the common potential function μ_m, and thus we have

$$\begin{aligned} &\mu_m^s\left(B_s^{t+1}, B_{-s}^t, \alpha_s^{t+1}, \alpha_{-s}^t\right) - \mu_m^s\left(B_s^t, B_{-s}^t, \alpha_s^t, \alpha_{-s}^t\right) \\ &\quad = \mu_m\left(B_s^{t+1}, B_{-s}^t, \alpha_s^{t+1}, \alpha_{-s}^t\right) \\ &\qquad - \mu_m\left(B_s^t, B_{-s}^t, \alpha_s^t, \alpha_{-s}^t\right), \forall\, s \in \wp. \end{aligned} \tag{38}$$

According to (37) and (38), we can come to a conclusion that each change of a player's strategy at each iteration will lead to a strict increasing quantity of μ_m. Since $\mu_m^* < \infty$, there must be t^* to meet $0 \leq t^* < \infty$ to make $\mu_m\left(B_s^{t^*}, B_{-s}^{t^*}, \alpha_s^{t^*}, \alpha_{-s}^{t^*}\right) = \mu_m^*$ when t^* is big enough. That is, the strict increasing process of the presented algorithm must converge in the finite steps. The proof is completed.

In Algorithm 2, the MBS firstly initializes each AP's access transmission duration and transmission power (see lines 1∼4). Secondly, it broadcasts its decision results to all the SITDs, and waits for all the SITDs to send their decision results (see lines 5∼7). Thirdly, it updates the transmission power and access transmission duration for each AP, and calculates its utility on the basis of formula (34) (see line 8). Finally, if the utility value could still be improved (see lines 16∼17), the second step and the third step are repeated (see lines 5∼15). It is noted that, in lines 10∼12, the MBS makes game decisions for all the APs in each game round, which is repeated if the utility value of any AP could still be improved (see lines 9∼15).

Algorithm 2: Iterative Algorithm to Get a Viable Strategy SNE.

Run at the MBS
Input: ε
Output: $\{B_s | s \in \wp\}$ and $\{\alpha_s^a | s \in \wp\}$
1: **For** $s \in \wp = \{1, 2, \ldots, S\}$ **do**
2: $\alpha_s^a \leftarrow \frac{1}{S_s} \in \Omega_t$
3: $B_s \leftarrow p_m^{t,K_m} \in P_m^t$
4: **End for**
5: $k \leftarrow 0$
6: Broadcast $[\{B_s | s \in \wp\}, \{\alpha_s^a | s \in \wp\}]^k$ to all the SITDs
7: Invoke Algorithm 1 to get $A_1 \times \ldots \times A_u \times \ldots \times A_U$
8: Compute the MBS's utility μ_m according to formula (34)
9: **Repeat**
10: **For** $s \in \wp$ **do**
11: $[B_s, \alpha_s^a]^{k+1} \leftarrow \text{argmax}_{B_s \in P_m^t, \alpha_s^a \in \Omega_t} [\mu_s]^{k+1}$
12: **End for**
13: $[\{B_s | s \in \wp\}, \{\alpha_s^a | s \in \wp\}]^k \leftarrow [\{B_s | s \in \wp\}, \{\alpha_s^a | s \in \wp\}]^{k+1}$
14: $k \leftarrow k + 1$
15: **Until** $[\mu_s]^k = [\mu_s]^{k-1}\ \forall s \in \wp$
16: **If** $\mu_m < [\mu_s]^k$ **then**
17: Go to 5
18: **Else**
19: Return
20: **End if**

D. Complexity Analysis for Proposed Scheme and Related Algorithms

We will do an analysis of the complexity of the proposed scheme in this subsection. Our scheme is referred as the relay-based hybrid resource allocation (RHRA) scheme according to its characteristics. In Algorithm 1 of RHRA, a player (i.e., SITD u) finding the NE needs to search $O(T_u H_u C_u)$, where T_u denotes the number of iterations executed by SITD u and C_u denotes a constant depending on the complexity of SITD u's computing the utility, while H_u denotes the search cost of SITD u in its action space during each iteration, and depends on the size of its action space Q_u as well as the search scheme. Because the action space is ordered, we use a binary search method, where the search overhead is $O(\log Q_u)$.

In Algorithm 2 of RHRA, a player (e.g., AP s) requires to search $O(T_s H_s C_s)$ for finding the NE, which is actually done by the MBS and thus the overhead is $O(\sum_{s=1}^{S} T_s H_s C_s)$ for all the APs. Here, T_s denotes the number of iterations executed by the MBS and C_s denotes a constant depending on the complexity of the MBS's computing the utility, while H_s denotes the search cost of the MBS's searching the action space of AP s during each iteration, which depends on the size of its action spaces Q_s^t and Q_s^α as well as the search method. Since each action space is ordered, we use a binary search method, where the search overhead is $O(\log Q_s^t + \log Q_s^\alpha)$.

Based on the above, the complexity of RHRA is $O(T_u H_u C_u) + O(\sum_{s=1}^{S} T_s H_s C_s)$, while the typical traditional exhaustive search method (e.g., a brute force approach) needs the overhead $O(\prod_{u=1}^{U} H_u C_u) + O(\prod_{s=1}^{S} H_s C_s)$ to search the NE. Therefore, RHRA can avoid enormous amount of computation when compared with the sequential (or exhaustive) search method under a huge number of APs and SITDs.

For the schemes (e.g., the centralized resource allocation (CRA) algorithm, the decentralized resource allocation (DRA) algorithm, the concurrent decentralized resource allocation (CDRA) algorithm in [9], and the multi-game-based hybrid resource allocation (MHRA) algorithm in [29]) closely related to RHRA in this article, the complexity of their algorithms is outlined below.

CRA is a centralized algorithm, which is executed by the MBS to make game decision for each game player including all the user terminals and APs. Therefore, the computational complexity of CRA finding the NE needs to search $O(T_c \sum_{k=1}^{U+S} H_k C_c)$, where T_c denotes the number of iterations executed by the MBS and C_c denotes a constant depending on the complexity of the MBS's calculating the utility, and H_k denotes the search cost of the MBS's searching the action space of game player k during each iteration, which depends on the size of its action space and the search algorithm. If game player k is a SITD, the size of its action space is K_{us}, while that is $S_s - 1$ if game player k is an AP. Because CRA does not specify a search algorithm, we use a binary search algorithm in its simulation, where the search overhead is $O(\log K_{us})$ or $O(\log(S_s - 1))$. With the expansion of network scale, the performance of the node executing CRA will become the bottleneck of the whole system.

DRA is a distributed algorithm and mainly involves game player selection, exploration, strategy updating. In game player selection, the MBS randomly selects a game player to calculates its utility, where the selected game player requires to exchange information with other game players by control plane. In exploration, the selected game player randomly selects another strategy and adheres to it during an estimation period to get the utilities calculated by other game players, which is in turn used to calculate its own utility. In strategy updating, the selected game player updates its strategy according to the predetermined rule. Therefore, the computational complexity of DRA finding the optimal NE needs $T_d(O(2C_{game}) + O(C_{upate}) + O(C_{sele}))$, in which C_{game} is a constant determined by the complexity of calculating the utility; C_{upate} is a small constant which represents the complexity of updating strategy selection procedure; C_{sele} is a small constant standing for the complexity of game player selection procedure; T_d denotes the number of iterations for DRA convergence.

CDRA is an improved version of DRA by considering a limited interference range resulting from the nature of high directional transmitting and high path loss in mmWave communications, which allows non-interfering players to simultaneously update its strategy at each iteration. Therefore, the computational complexity of CDRA finding the optimal NE needs $T`_d(O(2C`_{game}) + O(C`_{upate}) + O(C`_{sele}))$, in which the meanings of $C`_{game}$, $C`_{upate}$, and $C`_{sele}$ are same as those in DRA, and $T`_d$ is the number of iterations for CDRA convergence. Based on the algorithm design characteristics of DRA and CDRA, their convergence rate is orders of magnitude lower than that of CRA on relatively small network scale. With the expansion of network scale, the centralized execution game process of CRA will cause the convergence rate to gradually slow down, and the convergence rate advantage of CRA over DRA and CDRA will gradually shrink and may even be surpassed. In addition, in each game round of CRA, the order of game decision made by MBS for each player is fixed, which is not conducive to fully exploring the solution space to obtain a better solution. Because of the characteristics of randomly selecting players in each game round, DRA and CDRA are slightly superior to CRA in terms of network sum rate and network energy efficiency.

Like RHRA in this article, MHRA is a hybrid algorithm executed by the MBS and the access terminals. So the computational complexity of MHRA finding the optimal NE is the same as that of RHRA. Although the MBS and all the access terminals usually perform the corresponding part of MHRA alternately, each access terminal update its strategy independently and thus they can make its decision concurrently in theory. This characteristic of RHRA and MHRA determines that their convergence speed is at the same level as that of CRA on relatively small network scale. Because RHRA and MHRA are well adapted to the expansion of network scale, they will converge better than CRA when network scale is very large. As mentioned above, MHRA does not consider the relay-based backhaul resource allocation problem, and both the MBS and each access terminal aim at energy efficiency optimization, which cannot ensure that the data rate can be improved at any time while achieving better energy efficiency.

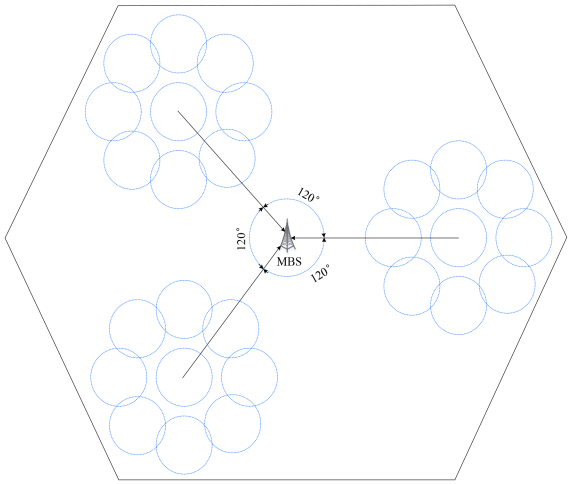

Fig. 4. mmWave access network simulation scenario.

TABLE I
SIMULATION PARAMETERS

Symbol	Description	Value
p_u^{max}	Maximum transmitting power for SITDs (Watts)	0.2
p_s^{max}	Maximum transmitting power for APs (Watts)	5
W	Unit resource block (or bandwidth) (GHz)	1
f_c	Carrier frequency (GHz)	28
B_m^r	Receiving beam width of the MBS from any AP	5°
B_s^t	Transmitting beam width of any AP to the MBS	2°~5°
B_s^r	Receiving beam width of any AP from any SITD	30°~90°
B_u^t	Transmitting beam width of any SITD to the associated AP	30°~90°
N_0	Thermal noise density (dBm/Hz)	−174
S_s	The number of time slices	20
K_{us}	The cardinality of the set P_{us}^t	50
K_m	The cardinality of the set P_m^t	500
P_{RF}	Power consumption of RF chain (Watts)	0.0344

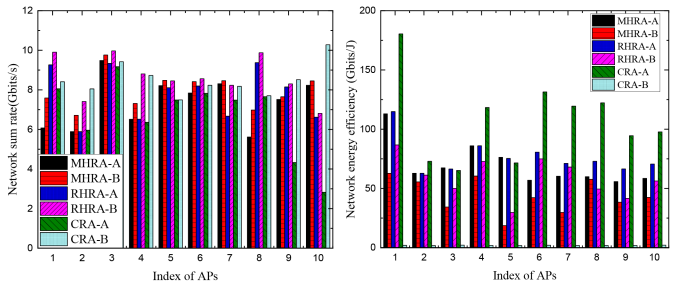

(a) (b)

Fig. 5. Performance comparisons of backhaul link and all access links per AP.

V. PERFORMANCE EVALUATION

A. Experimental Parameter Settings

The simulation experiments have been carried out to evaluate the performance of RHRA and the comparison algorithms (i.e., CRA and MHRA). As mentioned above, DRA and CDRA are slightly superior to CRA in terms of network sum rate and network energy efficiency, but they are far inferior to CRA in terms of convergence performance on a very small network scale. As described below, the network simulation scenario adopted in this article is relatively small in scale. In addition, the performance of DRA and CDRA in terms of network energy efficiency is much lower than that of MHRA. Therefore, DRA and CDRA are not selected for comparison in our simulation experiments.

Our simulation scenario mainly includes three clusters, whose characteristics are described in [11]. As shown in Fig. 4, three clusters are equally distributed around the MBS. According to the description of parameters in [9], the MBS's coverage radius is 500 m, the distance between the MBS and each cluster center is 150 m, and the cluster radius is 70 m. The distribution of APs within each cluster is similar to that shown in Fig. 1, where the radius of each AP is 20 m and the distance between any two APs is no less than 30 m. We implement the above simulation scenario and execute the simulation experiments in the event-based network simulator OMNeT++ (i.e., omnetpp-5.4.1). Each data point in the following simulation figures is the average value of 100 rounds of simulation results, where we only updated the random distribution of SITDs in each cluster in each round of simulation experiment.

To sum up, the Settings of our simulation parameters refer to [9], [11], where the main simulation parameters are shown in Table I. Unless stated specifically, the number, size, and orientation of beams at each AP are fixed.

B. Experimental Results and Analysis

We compare the performance metrics (i.e., network sum rate and energy efficiency) in different Settings of RHRA with various comparison algorithms. Then, we compare their convergent tendency. Next, we compare the effects of the maximum power level of each backhaul link, the beam width of transmitting/receiving beams, and the number of time slices per scheduling period on the performance metrics of RHRA. Finally, we compare the performance of RHRA with/without relay-assistance, and also show the effects of changes in the number of SITDs served by each AP on the performance of RHRA.

Fig. 5 shows the performance comparisons of the backhaul link and all the access links per AP of the three schemes with respect to network sum rate and network energy efficiency. Here, simulation environment is set up with 10 APs and each AP chooses 4 SITDs to serve. In Fig. 5, RHRA-B, MHRA-B, and CRA-B represent the backhaul performance per AP for RHRA, MHRA, and CRA, while RHRA-A, MHRA-A, and CRA-A represent the access performance per AP for RHRA, MHRA, and CRA, respectively. It is shown from Fig. 5(a) that each AP's backhaul capacity is always higher than its access capacity. This is because these schemes must meet the constraint that access data rate of each AP is not more than its backhaul capacity in the current scheduling period.

Fig. 5(a) shows that RHRA and MHRA have a better balance of access/backhaul data rate of each AP than CRA, while Fig. 5(b) shows that they have a much better balance of average energy efficiency between backhaul side and access side than CRA. The reasons behind the above phenomena are the reasonable power adjustment of each backhaul link in RHRA

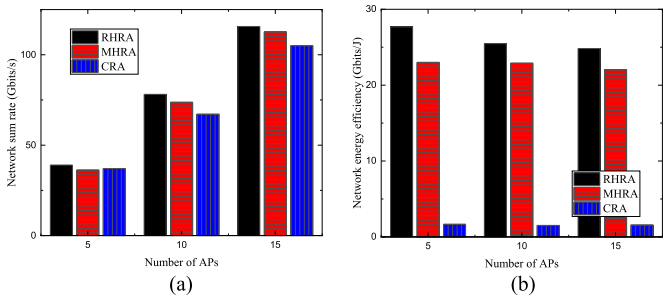

Fig. 6. Performance comparisons vs. the number of APs.

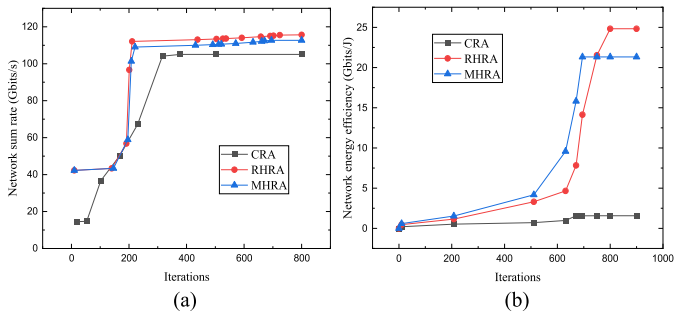

Fig. 7. Convergence behaviors of RHRA, MHRA, and CRA.

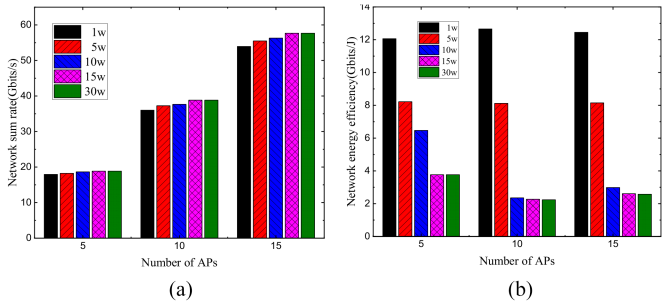

Fig. 8. Impact of maximum power level of each backhaul link on network performance metrics.

and MHRA. Furthermore, the power adjustment granularity of each backhaul link is coarser than that of each access link in RHRA and MHRA, resulting in a relatively poor network energy efficiency for each backhaul link. In particular, for each backhaul link in CRA, the transmission power is fixed at a relatively high value, resulting in a very poor network energy efficiency for each backhaul link.

Fig. 6 presents the comparisons among RHRA, MHRA, and CRA in terms of network sum rate and network energy efficiency. Here, the number of APs is set to 5, 10, and 15 respectively, and each AP chooses 4 SITDs to serve. We can observe that RHRA and MHRA outperform CRA in these performance metrics. Moreover, network energy efficiency of RHRA and MHRA has been greatly improved. This indicates that setting a backhaul power to consistency is unreasonable since there is a large difference in the length values of backhaul links. It is also noticed that network sum rate will increase with the number of APs, which is evident as the number of concurrent access links increases. At the same time, due to reasonable adjustment of transmission powers, the increasing number of concurrent links will not lead to the higher mutual interference. So the stability of energy efficiency of RHRA and MHRA can be maintained. As far as the comparison between RHRA and MHRA is concerned, the former is superior to the latter in terms of the performance metrics. The main reasons are obvious. Since RHRA adopts differentiated optimization goal design between the MBS and each access terminal and also considers the relay-based backhaul resource allocation problem, it is generally superior to MHRA in terms of network sum rate and network energy efficiency.

In order to compare the convergent tendency of RHRA with the other comparison algorithms, the metric definition of convergence should be clarified. In RHRA and MHRA, when the MBS selects an action policy and gets the feedback of all the SITDs' action policies, it is recorded as an iteration. When convergence is achieved, the number of iterations of RHRA, MHRA and CRA is on the same order of magnitude, which has been analyzed in detail in Section IV-D. On the contrary, whether it is the MBS or each SITD, it is recorded as an iteration as long as it selects an action policy. At this point, the number of iterations of RHRA and MHRA is more than that of CRA when convergence is achieved. In order to observe the convergence process at a finer granularity, the latter iteration definition is used in the following simulation experiments. Also, for fairness of convergence comparison among RHRA, MHRA and CRA, when the MBS executing CRA selects an action policy for anyone of all the APs and SITDs, it is recorded as an iteration.

Fig. 7 shows the convergence behaviors of RHRA, MHRA, and CRA in a multiple-cluster network with 15 APs and 60 SITDs. As can be seen from Fig. 7, network sum rate and network energy efficiency of RHRA, MHRA, and CRA will be updated in each iteration, and relatively stable suboptimal values are finally obtained. Meanwhile, it can be seen from Fig. 7 that RHRA and MHRA converges slightly faster than CRA. This phenomenon is attributable to the iteration definition adopted in the simulation of RHRA, MHRA, and CRA, as described above. The MBS executing CRA needs to select policies for all the APs and SITDs, while the MBS executing RHRA or MHRA only needs to select policies for all the APs. So the former records more iterations than the latter.

As mentioned earlier, when compared to the comparison algorithms, RHRA both adjusts relay-assisted backhaul transmission powers and adopts differentiated optimization goals for access terminals and network system, which is helpful to reduce mutual interference and unnecessary power consumption. So it achieves the better performance with respect to both network sum rate and network energy efficiency.

The maximum power level of each backhaul link, the beam width value of transmitting/receiving beams, and the number of time slices per scheduling period may affect the network sum rate and network energy efficiency. So we illustrate their influences on the performance metrics of RHRA, which are shown in Figs. 8–10. Here, the simulation environment is set up with 5, 10, 15 APs respectively and each AP chooses 2 SITDs to serve. Fig. 8 shows the performance metrics change with the number of APs under the different maximum power level of each backhaul

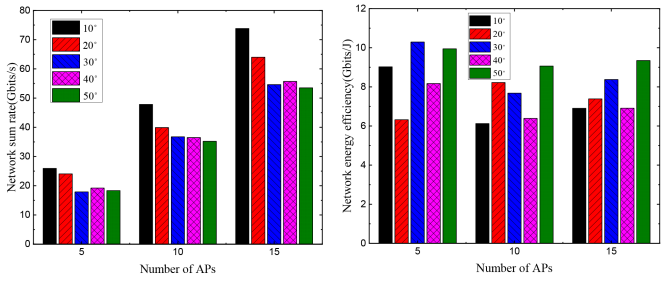

(a) (b)

Fig. 9. Impact of transmission beam width of SITDs and receiving beam width of APs on network performance metrics.

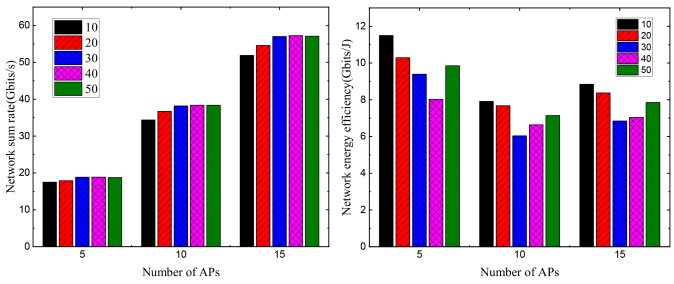

(a) (b)

Fig. 10. Impact of the number of time slices in each scheduling period on network performance metrics.

link. Here, the power level of each backhaul link can be adjusted to a range greater than 0 but no more than maximum backhaul power level.

We can see from Fig. 8(a) that, network sum rate increases significantly as the number of APs increases, while it increases slightly as the maximum power level increases. This is because the increase of APs will increase the number of concurrent access links. However, when the number of APs is fixed, the number of access links is also fixed in accordance with the foregoing Settings. So the change of backhaul power is the main factor affecting access data rate. When the backhaul transmission power is high enough, the benefit of further increasing its value is not obvious, and thus the network sum rate is basically unchanged.

We observe from Fig. 8(b) that network energy efficiency firstly decreases significantly and then basically keeps unchanged as the maximum power level increases. According to the above simulation environment Settings, the total data rate of the system is limited to the access data rate. Since the access data rate is basically unchanged, the increase of backhaul transmission power will reduce network energy efficiency. When the backhaul transmission power is further increased, most of the transmission time slices will be allocated to the access end in a scheduling period. So the average access data rate is increased, and thus the decline of network energy efficiency is slowed down.

In addition, when the maximum power level is fixed to a relatively small value (less than 10w), Fig. 8(b) shows that network energy efficiency is basically unchanged when the number of APs varies. Otherwise, Fig. 8(b) shows that network energy efficiency firstly decreases significantly and then basically keeps unchanged as the number of APs increases. The reason is due to the fact that the increase of concurrent links caused by the increase of APs will lead to different mutual interference under different backhaul powers. If a backhaul link uses more backhaul power, it benefits itself, but it also interferes more with the other backhaul links.

In the process of increasing transmission power for all the backhaul links, sometimes it is good but sometimes it is bad for system performance. When backhaul transmission power is relatively small, variation of mutual interference with the change of the number of APs may also be small. So network energy efficiency is basically unchanged. As the backhaul transmission power increases, the mutual interference will increase with the change of the number of APs. When the backhaul transmission power is increased further, the results may be reversed. Thus, the situation in Fig. 8(b) appears.

Fig. 9 shows the network performance metrics change with the transmission beam width of SITDs and the receiving beam width of APs. For simplicity and without loss of generality, we assume that all the SITDs have the same transmission beam width and all the APs have the same receiving beam width. In addition, all the APs have the same transmission beam width, which is fixed at 2° and aligned with the MBS, while the receiving beam width of the MBS is fixed at 5°.

Fig. 9(a) shows that network sum rate increases as the number of APs increases. But it decreases as the transmission beam width of SITDs and the receiving beam width of APs increases. The reason of the former is the same as the explanation for Fig. 8(a). But the reason of the latter is that the directional gain of each access link gets small when the transmission beam width of SITDs and the receiving beam width of APs increase. Fig. 9(b) shows that there is no obvious rule of change in terms of network energy efficiency when either the beam width size or the number of the APs varies. This may be due to the interaction of related factors such as the distribution of APs, the adjustable degree of each backhaul power, and differences of access data rates.

As can be seen from Fig. 10(a) that, network sum rate increases significantly with the number of APs, while it basically keeps unchanged or slightly increases as the number of time slices in each scheduling period increases. The reason of the former is the same as the explanation for Fig. 8(a), while the reason of the latter is that the more time slices will be helpful to get the more appropriate ratio of access transmission duration to backhaul transmission duration but the performance difference caused by different ratio value is not obvious.

We can also see from 10(*b*) that, as the number of time slices in each scheduling period increases, the network energy efficiency firstly tends to decline and then slightly increases. The reason is that the increasing number of time slices at least does not make network sum rate worse but it also does not guarantee a monotonous variation trend of each backhaul link's transmission power that meets data rate constraint between the access end and backhaul end.

Next, we give performance comparisons for RHRA with relay-assistance and RHRA without relay-assistance. Here, the number of APs is set to 3, 6, and 9 respectively, and each AP chooses 2 SITDs to serve. From Fig. 11, we see that RHRA with

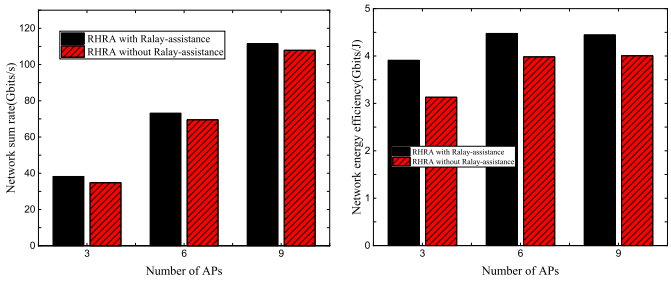

Fig. 11. Comparisons of impact of relay-assistance on RHRA.

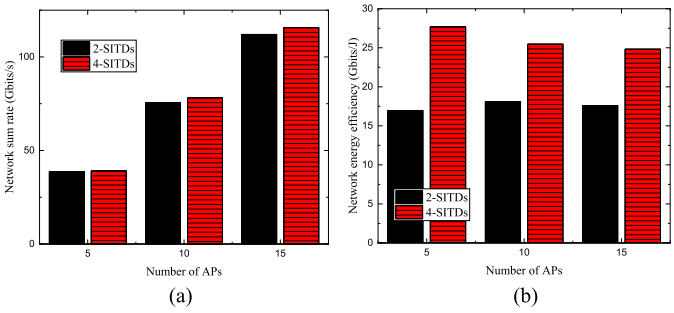

Fig. 12. Comparisons of impact of the number of served SITDs on RHRA.

relay-assistance is superior to RHRA without relay-assistance with respect to the network performance metrics. The main reason is explained as follows. In the case of space propagation with LOS condition, the channel gain is negatively correlated with the square of distance. With introduction of relay, it is possible to replace a very long communication link with two short LOS links, where channel attenuation can be effectively reduced and thus system performance can be improved. Moreover, we give performance comparisons for the two cases with two and four served SITDs for per AP in RHRA respectively, where the number of APs is set to 5, 10, and 15 respectively. As can be seen from Fig. 12, the case with 4-SITDs shows the better performance in terms of both network sum rate and network energy efficiency. The main reason is explained as follows. Under light access load, the requirement for backhaul capacity is relatively low, and the role of backhaul relay mode cannot be fully demonstrated.

Finally, we conduct statistical analysis on the variability of the three schemes. For simplicity without loss of generality, we use the simulation example in Fig. 6 to give the confidence intervals of each scheme for the two performance metrics at different simulation parameters, which means that at least 95% of the 100 data samples fall within the corresponding confidence interval. As shown in Table II, the small length of each confidence interval indicates that each scheme is not greatly affected by the random distribution change of SITDs.

VI. Conclusion

We address the problem of joint backhaul/access power adjustment and non-unified backhaul/access transmission duration allocation in a relay-assisted dense mmWave access network in this article, Firstly, to reduce the problem solving space, we decompose the problem concerned in this article into the data rate maximization sub-problem that each individual SITD wants and the energy efficiency maximization sub-problem that the entire network expects. Then, we further model the decomposed sub-problems as a Stackelberg game model. Finally, the extensive simulations show that the proposed RHRA outperforms the existing relevant schemes with respect to network sum rate and network energy efficiency.

TABLE II
Confidence Intervals of the Three Schemes

Scheme Name	Number of APs	Confidence Interval (Sum Rate; Energy Efficiency)
RHRA	5	([35.31,42.72];[25.05,30.31])
	10	([70.71,85.56];[23.05,27.89])
	15	([104.67,126.64];[22.47,27.18])
MHRA	5	([32.75,39.62];[20.82,25.19])
	10	([66.69,80.71];[20.71,25.06])
	15	([101.98,123.39];[19.94,24.12])
CRA	5	([33.51,40.55];[1.51,1.82])
	10	([60.76,73.52];[1.37,1.65])
	15	([95.08,115.05];[1.42,1.72])

References

[1] J. S. Gui, L. H. Hui, N. N. Xiong, and J. Wu, "Improving spectrum efficiency of cell-edge devices by incentive architecture applications with dynamic charging," *IEEE Trans. Ind. Informat.*, vol. 17, no. 2, pp. 795–808, Feb. 2021.

[2] X. Deng, Z. Sun, D. Li, J. Luo, and S. Wan, "User-centric computation offloading for edge computing," *IEEE Internet Things J.*, vol. 8, no. 16, pp. 12559–12568, Aug. 2021.

[3] Q. Zhang, W. Ma, Z. Feng, and Z. Han, "Backhaul-capacity-aware interference mitigation framework in 6G cellular Internet of Things," *IEEE Internet Things J.*, vol. 8, no. 12, pp. 10071–10084, Jun. 2021.

[4] K. Zheng, L. Zhao, J. Mei, M. Dohler, W. Xiang, and Y. Peng, "10 Gb/s HetSNets with millimeter-wave communications: Access and networking—Challenges and protocols," *IEEE Commun. Mag.*, vol. 53, no. 1, pp. 222–231, Jan. 2015.

[5] "Small cell backhaul requirements," NGMN Alliance, White Paper, Jun. 2012. [Online]. Available: www.ngmn.org

[6] M. Shariat, E. Pateromichelakis, A. u. Quddus, and R. Tafazolli, "Joint TDD backhaul and access optimization in dense small-cell networks," *IEEE Trans. Veh. Technol.*, vol. 64, no. 11, pp. 5288–5299, Nov. 2015.

[7] N. Wang, E. Hossain, and V. K. Bhargava, "Joint downlink cell association and bandwidth allocation for wireless backhauling in two tier HetNets with large-scale antenna arrays," *IEEE Trans. Wireless Commun.*, vol. 15, no. 5, pp. 3251–3268, May 2016.

[8] Y. P. Liu and X. M. Fang, "Joint user association and resource allocation for self-backhaul ultra-dense networks," *China Commun.*, vol. 13, no. 2, pp. 1–10, Feb. 2016.

[9] Y. Liu, X. Fang, and M. Xiao, "Discrete power control and transmission duration allocation for self-backhauling dense mmWave cellular networks," *IEEE Trans. Commun.*, vol. 66, no. 1, pp. 432–447, Jan. 2018.

[10] D. Monderer and L. S. Shapley, "Potential games," *Games Econ. Behav.*, vol. 14, no. 1, pp. 124–143, 1996.

[11] 3rd Generation Partnership Project (3GPP), "Small cell enhancements for E-UTRA and E-UTRAN—Physical layer aspects," 3GPP, Sophia Antipolis, France, Tech. Rep. 36.872, V.1.0.0, Rel.12, Aug. 2013.

[12] A. Mesodiakaki, F. Adelantado, L. Alonso, M. Di Renzo, and C. Verikoukis, "Energy and spectrum efficient user association in millimeter wave backhaul small cell networks," *IEEE Trans. Veh. Technol.*, vol. 66, no. 2, pp. 1810–1821, Feb. 2017.

[13] D. Fudenberg and J. Tirole, *Game Theory*. Cambridge, MA, USA: MIT Press, 1993.
[14] Z. Cui and R. Adve, "Joint user association and resource allocation in small cell networks with backhaul constraints," in *Proc. IEEE 48th Annu. Conf. Inf. Sci. Syst.*, 2014, pp. 1–6.
[15] U. Siddique, H. Tabassum, and E. Hossain, "Downlink spectrum allocation for in-band and out-band wireless backhauling of full-duplex small cells," *IEEE Trans. Commun.*, vol. 65, no. 8, pp. 3538–3554, Aug. 2017.
[16] C. Zhang, H. Wu, H. Lu, and J. Liu, "Throughput analysis in cache-enabled millimeter wave HetNets with access and backhaul integration," in *Proc. IEEE Wireless Commun. Netw. Conf.*, 2020, pp. 1–6.
[17] A. Chaudhari and C. S. R. Murthy, "Efficient dynamic relay probing and concurrent backhaul link scheduling for mmWave cellular networks," *Comput. Commun.*, vol. 149, pp. 146–161, Jan. 2019.
[18] Y. Niu et al., "Relay-assisted and QoS aware scheduling to overcome blockage in mmWave backhaul networks," *IEEE Trans. Veh. Technol.*, vol. 68, no. 2, pp. 1733–1744, Feb. 2019.
[19] G. Kwon and H. Park, "Beamforming design for low-power in-band wireless backhaul systems: Centralized and distributed approaches," *IEEE Trans. Veh. Technol.*, vol. 68, no. 2, pp. 1549–1563, Feb. 2019.
[20] G. Kwon and H. Park, "Joint user association and beamforming design for millimeter wave UDN with wireless backhaul," *IEEE J. Sel. Areas Commun.*, vol. 37, no. 12, pp. 2653–2668, Dec. 2019.
[21] M. Polese et al., "Integrated access and backhaul in 5G mmWave networks: Potential and challenges," *IEEE Commun. Mag.*, vol. 58, no. 3, pp. 62–68, Mar. 2020.
[22] S. Zhang, X. Xu, M. Sun, X. Tao, and C. Liu, "Joint spectrum and power allocation in 5G integrated access and backhaul networks at mmWave band," in *Proc. IEEE 31st Annu. Int. Symp. Pers., Indoor Mobile Radio Commun.*, 2020, pp. 1–7.
[23] X. Yuan, H. Tian, and G. Nie, "Joint access and backhaul link optimization in multiple UAV-assisted emergency network," in *Proc. IEEE/CIC Int. Conf. Commun. China*, 2020, pp. 735–740.
[24] A. Jain, E. Lopez-Aguilera, and I. Demirkol, "User association and resource allocation in 5G (AURA-5G): A joint optimization framework," *Comput. Netw.*, vol. 192, Jun. 2021, Art. no. 108063.
[25] Y. Niu et al., "Energy-efficient scheduling for mmWave backhauling of small cells in heterogeneous cellular networks," *IEEE Trans. Veh. Technol.*, vol. 66, no. 3, pp. 2674–2687, Mar. 2017.
[26] L. Chen, F. R. Yu, H. Ji, B. Rong, X. Li, and V. C. M. Leung, "Energy harvesting small cell networks with full-duplex self-backhaul and massive MIMO," in *Proc. IEEE Int. Conf. Commun.*, 2016, pp. 1–6.
[27] T. M. Nguyen, A. Yadav, W. Ajib, and C. Assi, "Centralized and distributed energy efficiency designs in wireless backhaul HetNets," *IEEE Trans. Wireless Commun.*, vol. 16, no. 7, pp. 4711–4726, Jul. 2017.
[28] X. W. Dai and J. S. Gui, "Joint access and backhaul resource allocation for D2D-assisted dense mmWave cellular networks," *Comput. Netw.*, vol. 183, Dec. 2020, Art. no. 107602.
[29] J. Gui, X. Dai, and N. N. Xiong, "Design and analysis of network behaviors for optimizing network energy efficiency in 5G mmWave systems," *IEEE Trans. Netw. Sci. Eng.*, vol. 8, no. 2, pp. 1842–1861, Apr.–Jun. 2021.
[30] N. Naderializadeh, J. J. Sydir, M. Simsek, and H. Nikopour, "Resource management in wireless networks via multi-agent deep reinforcement learning," *IEEE Trans. Wireless Commun.*, vol. 20, no. 6, pp. 3507–3523, Jun. 2021.
[31] L.-H. Shen and K.-T. Feng, "Mobility-aware subband and beam resource allocation schemes for millimeter wave wireless networks," *IEEE Trans. Veh. Technol.*, vol. 69, no. 10, pp. 11893–11908, Oct. 2020.
[32] O. Semiari, W. Saad, M. Bennis, and Z. Dawy, "Inter-operator resource management for millimeter wave multi-hop backhaul networks," *IEEE Trans. Wireless Commun.*, vol. 16, no. 8, pp. 5258–5272, Aug. 2017.
[33] P. Liu, J. Blumenstein, N. S. Perovi´c, M. Di Renzo, and A. Springer, "Performance of generalized spatial modulation MIMO over measured 60 GHz indoor channels," *IEEE Trans. Commun.*, vol. 66, no. 1, pp. 133–148, Jan. 2018.
[34] P. V. Amadori and C. Masouros, "Low RF-complexity millimeter-wave beamspace-MIMO systems by beam selection," *IEEE Trans. Commun.*, vol. 63, no. 6, pp. 2212–2222, Jun. 2015.
[35] W. Zhong, G. Chen, S. Jin, and K. K. Wong, "Relay selection and discrete power control for cognitive relay networks via potential game," *IEEE Trans. Signal Process.*, vol. 62, no. 20, pp. 5411–5424, Oct. 2014.
[36] S. Boyd and L. Vandenberghe, *Convex Optimization*. Cambridge, U.K.: Cambridge Univ. Press, 2004.

Jinsong Gui received the B.E. degree from the University of Shanghai for Science and Technology, Shanghai, China, in 1992, and the M.S. and Ph.D. degrees from Central South University, Changsha, China, in 2004 and 2008, respectively. He is currently a Professor with the School of Electronic Information, Central South University. His research interests include distributed systems, and related fields, such as wireless network topology control, cloud and green computing, and network trust and security.

Long Yin received the undergraduation degree from the School of Computer Science and Engineering, Central South University, Changsha, China. He is currently working toward the master's degree with the School of Computer Science and Engineering, Beihang University, Beijing, China. His research interests include Internet of Things and edge computing.

Xiaoheng Deng (Senior Member, IEEE) received the Ph.D. degrees in computer science from Central South University, Changsha, China, in 2005. He is a Senior Member of CCF, Member of CCF Pervasive Computing Council, and Member of IEEE and ACM. His research interests include wireless communications and networking, congestion control for wired/wireless network, cross layer route design for wireless mesh network and ad hoc network, online social network analysis, and edge computing.

Lin Cai (Fellow, IEEE) received the M.A.Sc. and Ph.D. degrees in electrical and computer engineering from the University of Waterloo, Waterloo, ON, Canada, in 2002 and 2005, respectively. Since 2005, she has been with the Department of Electrical and Computer Engineering, University of Victoria, Victoria, BC, Canada, and she is currently a Professor. She is an NSERC E.W.R. Steacie Memorial Fellow, an Engineering Institute of Canada Fellow, and a Canadian Academy of Engineering Fellow. In 2020, she was elected as a Member of the Royal Society of Canada's College of New Scholars, Artists and Scientists, and a 2020 Star in Computer Networking and Communications by N2Women. Her research interests include communications and networking, with a focus on network protocol and architecture design supporting emerging multimedia traffic and the Internet of Things. She has co-founded and chaired the IEEE Victoria Section Vehicular Technology and Communications Joint Societies Chapter. She has been elected to serve the IEEE Vehicular Technology Society Board of Governors, since 2019, and served its VP Mobile Radio, 2023. Since 2022, she has been a voting Board Member of IEEE Women in Engineering. She was an Associate Editor-in-Chief for IEEE TRANSACTIONS ON VEHICULAR TECHNOLOGY, a Member of the Steering Committee of IEEE TRANSACTIONS ON MOBILE COMPUTING, IEEE TRANSACTIONS ON BIG DATA, and IEEE TRANSACTIONS ON CLOUD COMPUTING, an Associate Editor for IEEE INTERNET OF THINGS JOURNAL, IEEE/ACM TRANSACTIONS ON NETWORKING, IEEE TRANSACTIONS ON WIRELESS COMMUNICATIONS, IEEE TRANSACTIONS ON VEHICULAR TECHNOLOGY, and IEEE TRANSACTIONS ON COMMUNICATIONS, and as the Distinguished Lecturer of the IEEE VTS Society and IEEE Communications Society.